



Using a composite flow law to model deformation in the NEEM deep ice core, Greenland: Part 1 the role of grain size and grain size distribution on the deformation of Holocene and glacial ice

Ernst-Jan N. Kuiper^{1,2}, Ilka Weikusat^{2,1,3}, Johannes H. P. de Bresser¹, Daniela Jansen², Gill M. Pennock¹,

5 Martyn R. Drury¹

¹Faculty of Earth Science, Utrecht University, 3508 TA Utrecht, the Netherlands

²Alfred Wegener Institute, Helmholtz Centre for Polar and Marine Research, 27570 Bremerhaven, Germany

³Department of Geosciences, Eberhard Karls University Tübingen, 72074 Tübingen, Germany

Correspondence to: E.N.Kuiper@uu.nl and M.R.Drury@uu.nl

10 **Abstract.** The effect of grain size on strain rate of ice in the upper 2207 m in the North Greenland Eemian Ice Drilling (NEEM) deep ice core was investigated using a rheological model based on the composite flow law of Goldsby and Kohlstedt (1997, 2001). The grain size was described by both a mean grain size and a grain size distribution, which allowed the strain rate to be calculated using two different model end members: (i) the micro-scale constant stress model where each grain deforms by the same stress and (ii) the micro-scale constant strain rate model where each grain deforms by the same strain rate. The model results show that basal slip accommodated by grain boundary sliding produces almost all of the deformation in the upper 2207 m of the NEEM ice core, while dislocation creep (basal slip accommodated by non-basal slip) hardly contributes to deformation. The difference in calculated strain rate between the two model end members is relatively small. The calculated strain rate in the fine grained glacial ice (1419-2207 m) varies strongly with depth and is about 4-5 times higher than in the coarser grained Holocene ice (0-1419 m). Two peaks in strain rate are predicted at about 1980 and 2100 m of depth. The results from the rheological model and microstructures in the glacial ice indicate that fine grained layers in the glacial ice will act as internal preferential sliding zones in the Greenland ice sheet.

1 Introduction

Ice sheets regulate global mean sea level (GMSL) by storing large amounts of fresh water in the form of ice on land. As a consequence of increased anthropogenic global warming, the contribution of the Greenland and the Antarctic ice sheet to GMSL rise is likely to increase in the next centuries (IPCC, 2014). It is therefore important to improve the implementation of ice flow in ice sheet models that calculate the discharge of ice into the ocean, since the amount of water stored in ice sheets is enough to raise GMSL by about 70 m (Alley et al., 2005; Church et al., 2013). The mass balance of an ice sheet depends on the accumulation of snow on the surface, release of meltwater by runoff and the solid discharge via floating ice shelves and calving of icebergs into the ocean (e.g. Petrenko and Withworth, 1999; Marshall, 2006). In the coldest parts of Antarctica,



sublimation and wind erosion can be important ablation mechanisms too (Bintanja, 2009). The amount of ice available for calving and melting depends on the flow of ice from the interior towards the margins of the ice sheet. This flow of ice is controlled by two processes: sliding of the ice over the bedrock, which includes various sub-glacial processes (Zwally et al., 2002; Vaughan and Arthern, 2007; Thoma et al., 2010; Wolovick and Creyts, 2016), and the internal deformation of the polycrystalline ice, which is governed by various mechanisms like dislocation creep, grain boundary migration (GBM) and grain boundary sliding (GBS) (e.g. Duval et al., 1983; Alley, 1992; Goldsby and Kohlstedt, 1997, 2001; Montagnat and Duval, 2000, 2004; Schulson and Duval, 2009; Faria et al., 2014a).

For large scale flow models, the deformation of the ice polycrystal is approximated in a homogenized way by continuum mechanics principles. Together with balance equations for mass, momentum and energy, continuum mechanics uses the relation between stress and strain rate given by a constitutive relation, also called the ‘flow law’. The most commonly used flow law in ice sheet models is Glen’s law (Glen, 1952, 1955; Paterson, 1994), which describes the flow of polycrystalline ice during deformation by a power law relating equivalent strain rate ($\dot{\epsilon}$) to equivalent stress (σ) according to

$$\dot{\epsilon} \propto \sigma^n, \quad (1)$$

where $n=3$ for Glen’s flow law. In this flow law, which is based on laboratory experiments, grain size insensitive (GSI) dislocation creep is assumed to be the dominant deformation mechanism. Variants of this type of strain rate-stress relation with different values for the stress exponent n have been used, ranging from $n=1.5$ to 4.0 , based on experiments at different conditions (Weertman, 1983). However, at the relatively low driving stresses of <0.3 MPa (equal to an equivalent stress of about 0.5 MPa using Equation 10) in terrestrial ice sheets (e.g. Sergienko et al., 2014), Glen’s flow law has proved to be inaccurate (e.g. Thorsteinsson et al., 1999; Huybrechts, 2007) and predicts strain rates that are too slow in both the deeper and the fine grained parts of the polar ice sheets. Laboratory experiments (Mellor and Testa, 1969a; Pimienta and Duval, 1987; Duval and Castelnaud, 1995; Goldsby and Kohlstedt, 1997, 2001; De La Chapelle et al., 1999; Duval et al., 2000) and flow analysis of ice sheets (Dahl-Jensen and Gundestrup, 1987; Alley, 1992) have shown that under these low stress conditions, ice deformation is best described by a flow law with a stress exponent less than 3.0 . However, most polar ice cores are drilled at low stress locations like domes or ridges (e.g. Faria et al., 2014b), where the ice might deform by different deformation mechanisms, and therefore be described by a different stress exponent than ice along the flanks or the margins of the ice sheet. The exact deformation mechanism of ice at these low driving stresses is still unclear.

During experiments with very fine grained ice (with a grain diameter between $3 \mu\text{m}$ and $90 \mu\text{m}$), Goldsby and Kohlstedt (1997) found a transition from a GSI creep regime with a power law stress exponent of $n=4$ at high equivalent stress ($\sigma > 3$ MPa) to a grain size sensitive (GSS) creep regime with $n=1.8$ and a grain size exponent of 1.4 at medium equivalent stress ($1-3$ MPa). At low equivalent stresses (<1 MPa) and with the finest grained samples, Goldsby and Kohlstedt found a third creep regime, again grain size independent, but with $n=2.4$. According to Goldsby and Kohlstedt, the GSI regime with $n=4$ is governed by dislocation creep using the easy slip systems in ice (basal slip) accommodated by the hard slip systems (i.e. non-basal slip). In the GSS regime with $n=1.8$, basal slip is thought to be accommodated by grain boundary sliding (GBS), while the opposite holds for the low stress GSI regime with $n=2.4$, where GBS is accommodated by basal slip. The



accommodating mechanisms are rate-controlling. At even lower stresses a fourth creep regime, diffusion creep, is expected. This creep regime is expected to dominate the flow behavior of ice at very small grain sizes ($\ll 1$ mm), low temperature and very low equivalent stresses. This creep regime was not reached during the experiments of Goldsby and Kohlstedt (2001) and is assumed to be irrelevant for terrestrial ice sheets (Goldsby and Kohlstedt, 2001; Durham et al., 2010). Therefore, diffusion
5 creep will not be considered in the remainder of this paper.

Goldsby and Kohlstedt (2001), Goldsby (2006) and Durham et al. (2010) suggested that Glen's flow law actually represents a combination of deformation mechanisms at the stress range 0.1-1.0 MPa (Glen, 1952, 1955), rather than only one deformation mechanism, that is, dislocation creep. This forms a possible explanation for a lack of accuracy found with Glen's flow law with fixed $n=3$ at very low stress (e.g. Peltier et al., 2000; Durham and Stern, 2001; Durham et al., 2010). For instance,
10 Schulson and Duval (2009) claim that the $n=4$ regime applies to tertiary creep, which was the same stress exponent found in the high pressure experiments by Kirby et al. (1987). Analysis also indicates that a power law with a stress exponent of $n=4$ describes best the observed state of the northern part of the Greenland ice sheet (Bons et al., 2018). Other factors that are often linked to polar ice being softer than predicted by Glen's flow law at low stress are the anisotropy of ice, impurity content and the softening of ice caused by a small grain size (e.g. Fisher and Koerner, 1986; Dahl-Jensen and Gundestrup, 1987; Paterson,
15 1991; Cuffey et al., 2000a). Attempts have been made to account for these softening factors by introducing a pre-exponential enhancement factor. When adjusted for anisotropy and grain size, this pre-exponential factor can be as high as 20 (Azuma, 1994). Instead of using an enhancement factor to artificially speed up Glen's flow law, a flow law of different nature may be used (Peltier et al., 2000).

The different GSS and GSI creep regimes recognized by Goldsby and Kohlstedt (1997, 2001) have been moulded by
20 these authors in the form of one composite flow law. The major advantage of such a composite flow law is that it explicitly denotes the components of the different creep mechanisms, rather than just describing bulk behaviour. This provides the opportunity to calculate the relative importance of the GSS and GSI deformation mechanisms over the range of temperatures, differential stresses and grain sizes found in ice sheets and compare their contribution to the total strain rate. This is not possible with the flow law developed by Baker (1981) for example, which adds a factor to the pre-existing Glen's flow law to account
25 for the effect of grain size.

It is well known that grain size varies throughout both the Greenland and the Antarctic ice sheets (e.g. Gow et al., 1997; Faria et al., 2014b; Binder, 2014; Fitzpatrick et al., 2014). However, the effect of grain size on strain rate is usually not considered in ice sheet models that apply flow laws of the type of Glen's flow law. Furthermore, the grain size is always expressed as a single mean grain size. However, small grains in a distribution might contribute differently to the overall
30 behaviour than large grains, with a given set of GSS and GSI mechanisms. Ter Heege et al. (2004) showed that using a mean grain size instead of a full grain size distribution in composite flow laws can lead to an over- or underestimate of the strain rates of natural rocks. In the NEEM ice core in northwest Greenland (77.45°N, 51.06°W, core length 2540 m) (NEEM community members, 2013), the dominant deformation mechanism in the Holocene ice is thought to be dislocation creep (e.g. De La Chapelle et al., 1998; Weikusat et al., 2017), while the microstructures in the glacial ice suggest that GSS mechanisms



may be important (e.g. Goldsby and Kohlstedt, 2002; Faria et al., 2014a). In this paper, the composite flow law is used to investigate the role of grain size on strain rate down to 2207 m of depth in the NEEM deep ice core and the results are compared to results obtained with Glen's flow law. The grain size data are described using both a mean grain size and a grain size distribution to evaluate the variation in grain size and the effect of grain size variation on strain rate in polar ice.

5 2 Methods

2.1 Study site and ice microstructure

The NEEM deep ice core was chosen because a comprehensive light microscope data set was available (Kipfstuhl, 2010) enabled by a fast line scan technique with microscopic resolution (LASM - Large Area Scanning Macroscope; Krischke et al., 2015). From these LM images the grain size distribution is available (Binder et al., 2013). The NEEM ice core was drilled
10 between 2008 and 2012 and is located close to an ice ridge (NEEM community members, 2013). The flow at the NEEM ice core is mainly parallel to the ridge with a small divergent component perpendicular to the line of the ridge (Montagnat et al., 2014). The top 1419 m of the NEEM deep ice core consists of ice deposited during the Holocene (Holocene ice), which shows a steadily increasing crystallographic preferred orientation (CPO) towards a vertical c-axis single maximum with a tendency towards a girdle (Eichler et al., 2013; Montagnat et al., 2014). The mean grain size increases from sub-millimetre size at the
15 surface to 3-4 mm at about 400 m of depth, after which it remains approximately constant for the remainder of the Holocene ice (Montagnat et al., 2014). At the transition from the Holocene ice to ice from the last glacial period (glacial ice), a sharp decrease in mean grain size to 1-2 mm is observed and the c-axis vertical clustering is further strengthened. At a depth of 2207 m, which is the transition from the glacial ice to the ice deposited during the Eemian period, the grain size increases sharply to tens of mm and the shape of the CPO varies strongly with depth (NEEM community members, 2013).

20 The difference in microstructure between the Holocene ice and the glacial ice of the NEEM ice core is shown in Figure 1. The Holocene ice core section (Figure 1a) was taken from a depth of 921 m and contains coarse grains with an aspect ratio of about 1:1 and has a relatively irregular grain boundary structure. The ice core section from the glacial ice (Figure 1b) is taken from a depth of 1977 m and is one of the finest grained ice core sections that was used in this study. The LM image shows very fine grained sub-horizontal bands with numerous quadruple junctions. The grains in these fine grained bands are
25 flattened and have an aspect ratio of about 2:1. The fine grained sub-horizontal bands contain many grains with aligned grain boundaries.

In this study, 615 LM images of the Holocene and glacial ice were used to determine the grain size evolution with depth in the NEEM ice core. These LM images were made of sections that were cut parallel to the long (vertical) axis of the ice core (Kipfstuhl et al., 2006). Each LM image is about 90 mm long and about 55 mm wide and was digitally analyzed using
30 the Ice-image software (www.ice-image.org) (Binder et al., 2013; Binder, 2014), which automatically detects the grain area of each grain in the cut sample surface by counting the pixels enclosed by grain boundaries. A lower cut-off grain size diameter



of 0.3 mm was used to exclude the small features that are produced as results of sample relaxation around air bubbles and segmentation by the analysis software (Figure 2).

2.2 The composite flow law

The composite flow law as proposed by Goldsby and Kohlstedt (2001) is formulated as follows:

$$\dot{\epsilon} = \dot{\epsilon}_{\text{disl}} + \left(\frac{1}{\dot{\epsilon}_{\text{basal}}} + \frac{1}{\dot{\epsilon}_{\text{GBS}}} \right)^{-1} + \dot{\epsilon}_{\text{diff}}, \quad (2)$$

where $\dot{\epsilon}$ is the total strain rate, composed of strain rates for basal slip accommodated by non-basal slip or dislocation creep, $\dot{\epsilon}_{\text{disl}}$, GBS accommodated by basal slip, $\dot{\epsilon}_{\text{basal}}$, and basal slip accommodated by GBS, $\dot{\epsilon}_{\text{GBS}}$, and diffusion creep, $\dot{\epsilon}_{\text{diff}}$. Each of these creep mechanisms can be described by a power law relation of the form:

$$\dot{\epsilon} = A \sigma^n d^{-p} \exp\left(-\frac{Q + PV^*}{RT}\right), \quad (3)$$

where A is a material parameter, σ is the differential stress (MPa), n is the stress exponent, d is the grain size diameter (m), p is the grain size exponent, Q is the activation energy for the creep mechanism at stake (J mol^{-1}), P is the hydrostatic pressure (MPa), V^* the activation volume ($\text{m}^3 \text{mol}^{-1}$), R is the gas constant ($\text{J K}^{-1} \text{mol}^{-1}$), and T the absolute temperature (K). The effect of PV^* is assumed to be very small (Durham and Stern, 2001) and is ignored for the remainder of this study. The power law relationship of Equation (3) also corresponds to the type of flow equation of Glen's law (Glen, 1955; Paterson, 1994).

As explained by Durham and Stern (2001), GBS and dislocation slip are sequential processes where the slowest mechanism determines the overall strain rate, i.e. is rate-limiting. Under the temperatures, grain sizes and stresses that occur in natural ice on Earth, basal slip will always give faster strain rates than GBS and non-basal slip (Goldsby and Kohlstedt, 2001; Goldsby, 2006). This makes, according to Goldsby and Kohlstedt (2001), either GBS or non-basal slip the accommodating (rate-limiting) mechanism for deformation of ice sheets. Therefore, basal slip-limited creep (GBS accommodated by basal slip) is not considered in the remainder of this paper, as this deformation mechanism is not relevant for polar ice sheets. Hence, the composite flow law simplifies to:

$$\dot{\epsilon} = \dot{\epsilon}_{\text{disl}} + \dot{\epsilon}_{\text{GBS}}. \quad (4)$$

Figure 3 shows the effect of grain size and stress on strain rate for Glen's flow law, GBS-limited creep, $\dot{\epsilon}_{\text{GBS}}$, and the dislocation creep mechanism, $\dot{\epsilon}_{\text{disl}}$, of the composite flow law. The chosen uniform temperature of 243K is representative for the upper 1200 m at NEEM (Sheldon et al., 2014). Glen's flow law and the dislocation creep mechanism are not dependent on grain size ($p=0$), but have a different slope to each other resulting from the different stress exponents. GBS-limited creep shows relatively fast strain rates at small grain sizes and low stresses. At higher stresses and larger grains, the dislocation creep mechanism is dominant over GBS-limited creep.

The smaller grains in a polycrystal can potentially deform by a different mechanism than the larger grains, since the smaller grains are more susceptible to GSS deformation mechanisms. In order to study the effect of the variation in grain size, a grain size distribution was used as well as a mean grain size in the flow law (Freeman and Ferguson, 1986; Heilbronner and Bruhn, 1998; Ter Heege et al., 2004). Similar to Freeman and Ferguson (1986) and Ter Heege et al. (2004), applying a grain



size distribution into a composite flow law leads to application of two theoretical end members to describe the deformation of ice: the homogeneous stress, or micro-scale constant stress model, and the homogeneous strain rate, or micro-scale constant strain rate model.

The micro-scale constant stress model assumes that each grain experiences the same stress, which is equal to the bulk stress of the material. However, the strain rate produced by each grain is different. The driving stress and the bulk strain rate produced by this model can be expressed as follows:

$$\sigma_{\sigma} = \sigma_1 = \sigma_2 = \sigma_i , \quad (5)$$

$$\dot{\epsilon}_{\sigma} = v_1 \dot{\epsilon}_1 + v_2 \dot{\epsilon}_2 + \dots + v_n \dot{\epsilon}_n = \sum_{i=1}^n v_i \dot{\epsilon}_i , \quad (6)$$

where the bulk volume has been segmented into n grain size classes, and v_i stands for the volume fraction of grain size class i , and $\dot{\epsilon}_i$ stands for the strain rate of grain size class i .

The micro-scale constant strain rate model assumes that each grain deforms by the same strain rate, which is equal to the strain rate of the bulk material. The stress required to produce this strain rate is different for each grain size class. This end member assumes that the larger grains in the polycrystalline material support more stress than the smaller grains and can be describes as follows:

$$\dot{\epsilon}_{\epsilon} = \dot{\epsilon}_1 = \dot{\epsilon}_2 = \dot{\epsilon}_i , \quad (7)$$

$$\bar{\sigma}_{\epsilon} = v_1 \bar{\sigma}_1 + v_2 \bar{\sigma}_2 + \dots + v_n \bar{\sigma}_n = \sum_{i=1}^n v_i \bar{\sigma}_i , \quad (8)$$

where $\bar{\sigma}_i$ stands for the stress supported by grain size class i . An iterative approach is required to calculate the strain rate when the bulk stress is known.

2.3 Boundary conditions and input data

The temperature in the NEEM borehole reaches 269.8K at the bedrock interface, which is only 0.9K below the estimated pressure-melting point (Sheldon et al., 2014). At this temperature it is expected that the deformation of ice is affected by premelting (e.g. Mellor and Testa, 1969b; Barnes et al., 1971; Morgan, 1991; Goldsby and Kohlstedt, 2001). To omit the effect of the different temperature thresholds given in Table 1 for Glen's flow law (263K), the GBS-limited mechanism (255K) and the dislocation creep mechanism (258K) of the composite flow law (Goldsby and Kohlstedt, 2001; Goldsby, 2006), the high temperature flow law parameters, and therefore the effect of premelting on strain rate, were not included in this study. Since the effect of premelting is expected to start close to the glacial-Eemian interface at about $T > 262K$ this paper (part 1) focuses on the relatively cold Holocene and glacial ice in the upper 2207m of NEEM. The deeper possibly premelted ice will be the subject of a companion paper (part 2), which will analyse the combined effects of grain size and premelting on deformation in the NEEM ice core.

The method of Heilbronner and Bruhn (1998) was used to convert 2D sectional areas to 3D volume fractions. This method uses an equivalent grain diameter that was determined for each grain and a 3D volume fraction was calculated with the assumption of a spherical grain. This method corrects for the over representation of small grains in an LM image compared to the bulk volume. The grain size distribution contains 80 grain size classes defined by steps of the equivalent diameter of 0.3



mm each, covering the full breath of the observed grain size distribution in the Holocene and glacial ice. The equivalent diameter of each grain in each ice core section was calculated and included in the corresponding grain size class. Figure 4 shows an example of the volume contribution of sectional circles and the corresponding volume contribution of spheres for an ice core section at 921 m of depth, (detail of microstructure is shown in Figure 1a).

5 The mean grain size (right panel of Figure 7c) was determined by dividing the total area, as classified by the “grain” category in the Ice-image software, by the number of grains for each LM image. This way, the areas affected by bubbles, fracturing or frost are excluded from the mean grain size calculation. A mean equivalent diameter for each ice core section was calculated by assuming a circular grain. When using a mean grain size, there are no series of volume fractions (Equation 6 and 8) so no application of the micro-scale constant stress model and the micro-scale constant strain rate model is required.

10

To calculate the strain rate using Glen’s flow law and the composite flow law at the location of the NEEM ice core, information about the variation of stress with depth in the ice sheet is required. As stress itself cannot be measured, the stress has to be estimated based on theoretical considerations and constraints on strain rates in the NEEM ice core.

15 The shear stress in an ice sheet is driven by gravity and is determined by the surface slope of the ice sheet and the depth from the surface z_{ice} . The shear stress along an ice core can be estimated using the shallow ice approximation (e.g. Hutter, 1983; Greve and Blatter, 2009):

$$\tau = -\rho_{ice} z_{ice} g \frac{\partial h}{\partial x}, \quad (9)$$

where τ is the shear stress (Pa), ρ_{ice} is the density of ice (910 kg m^{-3}), z_{ice} is the ice thickness (m), g is the gravitational constant (9.81 m s^{-2}) and $\frac{\partial h}{\partial x}$ is the surface slope in the direction of flow. The surface slope at NEEM is about 1.8 m km^{-1} (Montagnat et al., 2014) and the ice core length is 2540 m (Rasmussen et al., 2013). Assuming a constant ice density, the shear stress increases linearly with depth reaching 0.041 MPa at the ice-bedrock interface at NEEM. Both the composite flow law and Glen’s flow law were derived during uniaxial deformation tests in secondary creep (Glen, 1952, 1955; Goldsby and Kohlstedt, 1997, 2001). So in order to use the shear stress as input for the flow laws, the shear stress has to be converted to an equivalent stress σ_e using the following relationship (Paterson and Olgaard, 2000):

25
$$\sigma_e = \sqrt{3} \tau, \quad (10)$$

which results in an equivalent axial differential stress at the ice-bedrock interface at NEEM of 0.071 MPa as shown in Figure 5.

30 The upper part of the NEEM ice core is dominated by longitudinal stress, perpendicular to the plane of the divide, leading to thinning of the annual layers (Dansgaard and Johnsen, 1969; Montagnat et al., 2014). Longitudinal stresses can be calculated from the increase of the ice slope away from the divide, if the rheology of ice is assumed (Raymond, 1983; Dahl-Jensen, 1989a). In this study, the simple approach of assuming an imposed stress-depth relationship will be taken to investigate how ice rheology is influenced by grain size, temperature and imposed stress. The layer thinning in the upper part of an ice core provides a constraint on the vertical strain rate, which in case of the NEEM ice core gives a value of about $3.2 \cdot 10^{-12} \text{ s}^{-1}$



(Gillet-Chaulet et al., 2011; Montagnat et al., 2014) in the Holocene ice. This strain rate can be used to estimate the equivalent stress in the upper part of the ice sheet using the composite flow law and Glen's flow law (Figure 5). A constant equivalent stress value of 0.07 MPa using the composite flow law, reproduced the rate of observed layer thinning, as shown in Figure 8. (Note that Figure 8 is based on the composite flow law with the modified flow law parameters, discussed in section 3). For
5 Glen's flow law the equivalent stress required to reproduce the observed layer thinning in the Holocene ice is lower at about 0.04 MPa. It was therefore decided to assume a constant equivalent stress of 0.07 MPa along the length of the NEEM ice core as input for Glen's flow law and the composite flow law. At the base of the ice sheet the vertical equivalent stress will tend to zero, with the decrease of vertical stress depending on the stress exponent in the flow law (Dansgaard and Johnson, 1969; Dahl-Jensen, 1989b).

10 The assumption of constant equivalent stress with depth is not realistic for ice sheets in general (e.g. Dahl-Jensen, 1989b). However, this assumption is a useful first approximation for the NEEM ice core where the equivalent stress, related to the shear stress in the lower part of the ice core, is by coincidence similar to the magnitude of equivalent stress related to the vertical stress in the upper part of the ice core. As this paper explores the effect of grain size, grain size distribution and different micro-scale models on the dominant deformation mechanism and the total strain rate, it is beyond the scope of this
15 study to derive a stress-depth model for NEEM because this requires knowledge on the rheology, which is the property that is investigated here. When calculating strain rates, no distinction is made between simple shear and pure shear deformation.

3 Flow law parameters

The original flow law parameters for the simplified composite flow law (Goldsby, 2006) and Glen's flow law (Paterson, 1994) are given in Table 1 for low temperatures where no premelting effects are expected. In order to apply the composite flow law
20 of Goldsby and Kohlstedt (2001) to the NEEM ice core, a check was made of the various published flow laws (Goldsby and Kohlstedt, 1997, 2001; Goldsby, 2006) with the experimental data. A comparison of the calculated strain rate for dislocation creep with the experimental data points from Figure 6 of Goldsby and Kohlstedt (2001) was made. The calculated strain rates were based on the flow law parameters in Table 1 and using Equation (3). This comparison is shown in Figure 6a. The solid
25 blue line shows the calculated strain rate for dislocation creep when the flow law parameters of Table 1 were used and forced with a stress of 6.3 MPa, which is the same stress as used in Figure 6 of Goldsby and Kohlstedt (2001). The calculated strain rate does not coincide with the three experimental data points for a temperature of $<258\text{K}$. The calculated strain rate is about 15 to 20 times higher than the experimental strain rates. An Arrhenius plot for GBS-limited creep (Figure 6b) was also calculated using a stress of 0.53 MPa and a uniform grain size of $73\ \mu\text{m}$, similar to Figure 4 of Goldsby and Kohlstedt (2001) and using the flow law parameters of Table 1. For this deformation mechanism, the calculated strain rate agrees well with the
30 experimental data points at $T < 255\text{K}$ of Goldsby and Kohlstedt (2001).

To account for the discrepancy between the dislocation creep mechanism and the experimental data, the flow law parameters were modified (dashed blue line, Figure 6a). The modified flow law parameters that are proposed here are shown



in Table 2. For GBS-limited creep, the flow law parameters remain the same as in Table 1. However, for dislocation creep, the material parameter A and the activation energy Q (Table 2) change significantly compared to the values given by Goldsby and Kohlstedt (2001) and Goldsby (2006) shown in Table 1. These modified flow law parameters show a better agreement with the experimental data points for dislocation creep at $T < 258$ (Figure 6a).

5 4 Results

Figure 7 shows plots of the equivalent strain rate as a function of depth for Glen's flow law and the composite flow law with its two different deformation mechanisms and the three different model end members calculated using the original flow law parameters (Table 1). The contribution of GBS-limited creep to bulk strain rate is also shown. The temperature input for all the models is shown in the right panel of Figure 7c. The results using the full grain size distribution with the micro-scale constant stress model (Figure 7a) and the micro-scale constant strain rate model with the grain size distribution (Figure 7b) are shown, as well as the results using the mean grain size model (Figure 7c) and the mean grain size evolution with depth (right panel of Figure 7c). All models show similarities, such as (i) a relatively constant strain rate between 400 m and 1400 m of depth, (ii) a strain rate increase below 1400 m of depth and (iii) a higher strain rate for Glen's flow law compared to the composite flow law along the entire depth range down to 2207 m of the NEEM ice core. In all of the three model end members, the calculated strain rate for GBS-limited creep and the composite flow law both show a more variable strain rate below 1400 m. This depth coincides with the transition from the coarse grained Holocene ice to the finer grained glacial ice and with an increase in temperature (Figure 7c, right panel). The peak values in strain rate in the glacial ice, indicated by the arrow in Figure 7a, predict strain rates that are comparable to the strain rate calculated using Glen's flow law. Two strain rate peaks occur at about 1980 m and 2100 m of depth and show a two to three-fold increase in strain rate compared to the mean strain rate in the glacial ice predicted by the composite flow law.

Throughout most of the Holocene ice (above 1419 m of depth), the dislocation creep (basal-slip accommodated by non-basal slip) mechanism predicts a slightly higher strain rate than the GBS-limited creep (basal-slip accommodated by GBS) mechanism for each of the three models. The difference between the strain rates of GBS-limited creep and dislocation creep in the Holocene ice is smaller for the micro-scale constant stress model than for the micro-scale constant strain rate model and the mean grain size model. In the glacial ice, dislocation creep and GBS-limited creep have roughly the same strength for each of the three models, apart from the higher variability in strength of the GBS-limited creep with depth. Compared to the micro-scale constant stress model, the micro-scale constant strain rate model predicts slightly lower absolute strain rates from GBS-limited creep along the entire upper 2207 m of depth of the NEEM ice core (Figure 7a, b) and especially below 1419 m of depth where the strain rate is more variable. The average strain rate predicted by the composite flow law is 10% higher in the glacial ice and 8% higher in the Holocene ice when using the micro-scale constant stress model instead of the micro-scale constant strain rate model. Using a mean grain size produces a weaker variability in strain rate with depth than the two model end members using a grain size distribution (Figure 7c).



Figure 8 is similar to Figure 7, but shows the results for the NEEM ice core using the modified flow law parameters (Table 2). The trends are similar to those in Figure 7, with the main difference that dislocation creep hardly contributes to the overall strain rate for each of the three models. Using the modified flow law parameters (Figure 8a-c), the three models predict that almost all deformation in the upper 2207 m of depth in the NEEM ice core is produced by GBS-limited creep. The strain rate peaks in the glacial ice at a depth of about 1980 and 2100 m are slightly weaker than the peaks calculated with the original flow law constants (Table 1) in Figure 7. The average strain rate in the Holocene ice is about 60% higher using the micro-scale constant stress model compared to the micro-scale constant strain rate model. For the glacial ice, this difference between the two model end members is about 40%.

Figure 9a and 9b show the strain rate per grain size class and the contribution of the two deformation mechanisms (Equation 4) for an ice core section at 921 m of depth. Part of this ice core section is shown in Figure 1a. This ice core section is located in the middle of the Holocene ice and has a relatively high variation in grain size. Since dislocation creep is a GSI mechanism, the strain rate produced by this deformation mechanism is the same for each grain size class in the micro-scale constant stress model (Figure 9a). GBS-limited creep shows faster strain rates than dislocation creep and strongly decreases in strain rate with increasing grain size, which is consistent with the inversely relationship to grain size given in Equation (3). The volume contribution of each grain size class (black bars in Figure 9a and 9b) is used in Equation (6) to calculate the bulk strain rate for this ice core section and in Equation (8) to iteratively calculate the stress supported by each grain size class.

The total strain rate produced by each grain size class is set to be the same for the micro-scale constant strain rate model shown in Figure 9b. The relative contribution of each deformation mechanism differs between grain size classes. GBS-limited creep is the dominant deformation mechanism for the smallest grains, whereas dislocation creep becomes increasingly more important for classes with larger grain sizes. However, even for the largest grains in this ice core section the strain rate produced by GBS-limited creep is still slightly larger than the strain rate produced by dislocation creep.

The stress supported per grain size class for the micro-scale constant stress and micro-scale constant strain rate model for the composite flow law is shown in Figure 9c. The stress supported per grain size class using the micro-scale constant strain rate model is used in Equation (8) to iteratively calculate the stress in the bulk material of the ice core section. The smallest grain size classes support only a small amount of stress, since they are more sensitive to GBS-limited creep. As a consequence, the larger grains support more stress and activate a significant amount of dislocation creep.

To study the dominant deformation mechanism of the composite flow law at different stress levels as well as its comparison in strain rate to Glen's flow law, both flow laws were forced at different stress values, which roughly cover the range of equivalent stresses in the Greenland and Antarctic ice sheets (Sergienko et al., 2014). Figure 10a shows the calculated strain rate for dislocation creep and GBS-limited creep using the grain size distribution with the micro-scale constant stress model and the temperature profile of NEEM, forced with different constant stress values. At the lowest stress of 0.01 MPa, the strain rate produced by dislocation creep is about three orders of magnitude lower than the strain rate produced by GBS-limited creep. With increasing stress, the contribution of dislocation creep to the overall strain rate becomes bigger and at a stress of 0.25 MPa, dislocation creep and GBS-limited creep have roughly the same strength. The strain rate produced by the dislocation



creep mechanism at 0.50 MPa is roughly five times higher than for GBS-limited creep. A similar graph showing the calculated strain rate for the composite flow law and Glen's flow law is shown in Figure 10b. At the lowest stress of 0.01 MPa the composite flow law predicts a slightly higher strain rate compared to Glen's flow law. However, with increasing stress, Glen's flow law predicts progressively higher strain rates than the composite flow law. At the highest stress of 0.50 MPa, the strain rate predicted by Glen's flow law is almost an order of magnitude higher than the strain rate predicted by the composite flow law.

5 Discussion

In the first part of the discussion, the results obtained using the original flow law parameters (Figure 7) and the modified flow law parameters (Figure 8) are discussed. Emphasis is given to the results obtained using the modified flow law parameters (Table 2), as these parameters show a better fit with the experimental data points than the original flow law parameters from Goldsby (2006) (Table 1). The modification is the most straightforward solution to account for the inconsistency between given parameters (Table 5 in Goldsby and Kohlstedt, 2001) and experimental results (Figure 6 in Goldsby and Kohlstedt, 2001). The modification of the flow law parameters results in dislocation creep being about 15 to 20 times slower compared to the original flow law parameters.

5.1 Comparison of micro-scale constant stress versus micro-scale constant strain rate model

The main difference between the micro-scale constant stress model and the micro-scale constant strain rate model is that the micro-scale constant stress model allows the smallest grains to deform more than an order of magnitude faster than the larger grains (Figure 9a), while this is not possible in the micro-scale constant strain rate model (Figure 9b). For the micro-scale constant strain rate model, the strain rate is set to be the same for each grain size class. GBS-limited creep and dislocation creep are therefore co-dependent, since the sum of the two deformation mechanisms has to add up to a certain strain rate (Equation 4). Consequently, since the strain rate produced by GBS-limited creep decreases with increasing grain size, the contribution of dislocation creep to bulk strain rate increases with grain size. This effect is shown in Figure 9b where the bulk strain rate is similar for each grain size class, but the contribution of dislocation creep to the bulk strain rate increases with increasing grain size. Due to this co-dependence of dislocation creep and GBS-limited creep in the micro-scale constant strain rate model, the strain rate produced by dislocation creep varies slightly with depth as is shown in Figure 7b and 8b.

For most ice core samples, the finest grain size classes contribute only slightly to the bulk volume of the material, as is also the case for the ice core section at 921 m of depth shown in Figure 9. For this particular ice core section, the smallest grain size classes (<0.9 mm) make up only 2.7% of the bulk volume. Therefore, the contribution of these smallest grain size classes to the bulk strain rate remains limited. Nevertheless, the average strain rate in the Holocene ice calculated using the micro-scale constant stress model and the modified flow law parameters (Table 2) is 60% higher than the average strain rate produced by the micro-scale constant strain rate model. In the glacial ice, where the grain sizes are finer and grain size



distributions are more uniform, the difference in strain rates between the micro-scale constant stress and micro-scale constant strain rate model is 40%. However, these differences are remarkably small compared to results obtained for the two model end members in wet olivine (Ter Heege et al., 2004) and calcite mylonites (Herwegh et al., 2005). In wet olivine, the bulk strain rate could be up to an order of magnitude higher for the micro-scale constant stress model compared to the micro-scale constant strain rate model for samples with a high standard deviation in grain size distribution. This indicates that the grain size variation measured within each of the 90 x 55 mm ice core sections is not large enough to change the strain rate by an order of magnitude as observed for wet olivine.

By assuming that each grain deforms by the same amount in the micro-scale constant strain rate model, the strain heterogeneities that have often been observed in ice core microstructures (e.g. Obbard et al., 2006; Weikusat et al., 2009a; Faria et al., 2014a; Piazzolo et al., 2015; Jansen et al., 2016) are ignored. Contrary to the micro-scale constant stress model, where the contribution of the finest grains is relatively large compared to their volume contribution, the micro-scale constant strain rate model likely overestimates the role of the larger grains on the bulk strain rate in the ice core section. Therefore, the two models represent the lower and upper limit of deformation behavior of a polycrystal with a distributed grain size (Ter Heege et al., 2004).

5.2 comparing grain size distribution model end members with the mean grain size model

The difference in calculated strain rate between using a grain size distribution with the micro-scale constant strain rate model and the mean grain size model is relatively small (Figure 8b and c). A single mean grain size eliminates the effect that smaller grains have on the bulk strain rate. However, the effect of the smaller grains on strain rate in the micro-scale constant strain rate model is also limited since all grain size classes deform by the same amount and thus the difference in bulk strain rate between the micro-scale constant strain rate model and mean grain size model is small. The much larger computational expense of the micro-scale constant strain rate model and the small difference in calculated strain with the mean grain size model argues for using a mean grain size model over a micro-scale constant strain rate model when modelling GSS behaviour in polar ice sheets.

The difference in calculated strain rate between the micro-scale constant stress model and using a mean grain model size is larger than the difference between the micro-scale constant strain rate model and the mean grain size model. The strain rate peaks predicted in the layers at about 1980 m and 2100 m of depth are two to three times larger for the micro-scale constant stress model compared to the mean grain size model (Figure 8a, c). This difference is mainly caused by the effect that the finest grains have on the bulk strain rate in the micro-scale constant stress model (Figure 9a).

5.3 Stress sensitivities

Figure 10a shows that, at equivalent stresses below 0.25 MPa, the strain rate produced by GBS-limited creep is higher than the strain rate produced by dislocation creep, while at an equivalent stress of 0.50 MPa the strain rate produced by dislocation creep is higher than GBS-limited creep. The stress sensitivity of dislocation creep is controlled by a stress exponent of $n=4$,



while the stress sensitivity of GBS-limited creep is controlled by $n=1.8$. Thus, if temperature and grain size remain constant, dislocation creep becomes progressively stronger relative to GBS-limited creep with increasing stress. However, with the temperature profile and grain size data from the upper 2207 m of depth in the NEEM ice core, an equivalent stress of about 0.25 MPa is required for dislocation creep to become as strong as GBS-limited creep. Such a high stress is not reached in the NEEM ice core as the best estimate gives an equivalent stress of 0.07 MPa. However, the driving stress progressively increases from the ice domes and divides towards the margins of the ice sheet, reaching a driving stress of about 0.30 MPa at the margins of the ice sheets (Sergienko et al., 2014). A driving stress of 0.30 MPa corresponds to an equivalent stress of about 0.50 MPa (Equation 10). Therefore, if the temperature and grain size along the NEEM ice core is comparable to the ice along the margins of the ice sheet, the dominant deformation mechanism could switch from GBS-limited creep near domes and divides to dislocation creep near the margins of the ice sheets.

Interestingly, the stress of 0.10-0.50 MPa is within the range of stresses (0.1-1.0 MPa) that was used during the deformation experiments of Glen (1952, 1955). The grain size reported of 1-2 mm by Glen (1952) is similar to the grain size in the glacial ice of the NEEM ice core (Figure 8c, right panel). The results in Figure 10a for 0.25 MPa show that the contribution of dislocation creep and GBS-limited creep to the total strain rate in the glacial ice is roughly equal. This result supports the hypothesis of Durham et al. (2001), Goldsby and Kohlstedt (2001, 2002) and Goldsby (2006) that the stress exponent of $n=3$ found by Glen (1952, 1955) is the result of collecting data at a transition regime between $n=4$ for dislocation creep and $n=1.8$ for GBS-limited creep.

Comparison of the results using the composite flow law with Glen's flow law at different equivalent stresses (Figure 10b) shows that at a stress of 0.01 MPa the composite flow law predicts a higher strain rate than Glen's flow law in most of the upper 2207 m of depth in the NEEM ice core. In the finest grained parts of the glacial ice, the composite flow law predicts a strain rate that is about five times faster than predicted by Glen's flow law at the low equivalent stress of 0.01 MPa. As the equivalent stress increases, Glen's flow law becomes progressively faster relative to the composite flow law. Since the dominant deformation mechanism of the composite flow law at low equivalent stress is GBS-limited creep (Figure 10a), the effective stress exponent will also be close to the stress exponent for GBS-limited creep ($n=1.8$). Glen's flow law, driven by a stress exponent of $n=3$, shows therefore a stronger increase in strain rate with increasing stress than the composite flow law. Consequently, at a driving stress of 0.25 MPa, Glen's flow law predicts a strain rate that is about an order of magnitude faster than the strain rate predicted by the composite flow law. As the contribution of dislocation creep in the composite flow law increases with increasing stress (Figure 10a), the sensitivity of the bulk strain rate to grain size variation decreases with increasing stress since dislocation creep is insensitive to grain size. This effect can be seen in Figure 10b where the strain rate peaks and the layer-to-layer variability predicted by the composite flow law become weaker with increasing stress.

5.4 Variability of predicted strain rates with depth

Levels of high borehole closure and borehole tilting have been observed in many polar ice cores and often coincide with high impurity content and small grain sizes (e.g. Fisher and Koerner, 1986; Paterson, 1994). These depth levels can be seen as layers



with a different microstructure than the surrounding ice and therefore deform at a higher strain rate. The reason that small grain size and high impurity content coincide is still not well understood (Eichler et al., 2017). The results using the composite flow law suggest that prominent soft layers, i.e. layers with a high strain rate, could be present at two depths of about 1980 and 2100 m in the NEEM ice core. These soft layers are located in the lower part of the NEEM ice core, which is dominated by simple shear (Dansgaard and Johnson, 1969; Montagnat et al., 2014). The soft layers can therefore be seen as depths where a high rate of simple shear occurs, instead of layers with enhanced extrusion (Waddington, 2010). However, it is likely that not all soft layers that are caused by finer grains have been identified since the available sampling rate of 615 LM images along 2207 m of depth of the NEEM ice core leaves many depth intervals not studied. Glen's flow law is unable to predict soft layers related to grain size variations since the flow law is forced by stress and temperature only. The effects of anisotropy, grain size and/or impurity content on strain rate are often incorporated in the form of an enhancement factor (Azuma, 1994; Thorsteinsson et al., 1999). However, information about the softening effects, like grain size, are needed in order to incorporate the enhancement factor with the right value and at the right depth. This can only be achieved by a flow law that explicitly describes GSS deformation, such as the composite flow law of Goldsby and Kohlstedt (2001).

Another reason why soft layers might have been missed during this study is that by taking the grain size distribution of the 90 x 55 mm LM images, the fine grain size of shear bands or cloudy bands (Faria et al., 2010; 2014a) could have been averaged out. Often, these bands have a vertical thickness that is much thinner than the 90 mm height of the LM images (see examples in Figure 1b; Figure 4 in Faria et al., 2014b). Therefore, it is likely that many soft layers in the glacial ice of the NEEM ice core have not been identified in this study or have been averaged out over the 90 x 55 mm LM images.

5.5 Microstructural evidence and CPO development

The c-axis eigenvalues show a minor variability in the glacial ice of the NEEM ice core (Eichler et al., 2013; Montagnat et al., 2014) where the layers of high strain rate are predicted. The strong development of CPO and the development of substructures with depth indicate that large amounts of strain are accommodated by basal slip of dislocations in the NEEM ice core. This may seem to be in disagreement with the conclusion that GBS-limited creep is the dominant deformation mechanism. However, grain boundary sliding is assumed to be the accommodating mechanism, with basal slip being the main strain producing mechanism. Several studies on minerals such as calcite (Schmid et al., 1987; Rutter et al., 1994), olivine (Drury et al., 2011; Hansen et al., 2011, 2012) and the rock analogue octachloropropane (Bons and Jessell, 1999) have shown that a CPO can develop in materials deforming by GSS deformation alone or in combination with GSI deformation. A modelling study of Zhang et al. (1994) showed that, if the amount of grain boundary sliding relative to intracrystalline slip is small, even stronger CPOs are developed compared to simulations where no grain boundary sliding was allowed. If indeed CPO in polar ice can be strengthened by a grain size sensitive deformation mechanism, then this could partly explain the sudden jump in CPO strengthening at the Holocene-glacial transition in the NEEM ice core (Eichler et al., 2013; Montagnat et al., 2014). This jump in CPO coincides with the enhanced GBS-limited creep at the Holocene-glacial transition as shown in Figure 8. The high strain rates produced by GBS-limited creep at a depth of about 1980 and 2100 m also correspond with the highest c-axis eigenvalues



in the NEEM ice core of >0.95 (Eichler et al., 2013; Montagnat et al., 2014). For example, the very fine grained ice core section at a depth of 1977 m, part of which is shown in Figure 1b, has a CPO with a first eigenvalue of 0.97.

For both the composite flow law and Glen's flow law, the influence of CPO on strain rate is not taken into account during this study, for example by a pre-exponential enhancement factor. In simple shear, a strong single maximum CPO produces less strain incompatibilities at grain boundaries by aligning the basal planes of the ice crystals in the direction of the flow. This means that less accommodation of basal slip is required by either non-basal slip or GBS per unit of strain, which causes the strain rate to increase compared to an isotropic ice sample. The strain rate enhancement caused by a well-developed CPO is about 2.3 times stronger in simple shear than in pure shear (Budd and Jacka, 1989; Treverrow et al., 2012). Therefore, the difference in equivalent strain rate between the Holocene and the glacial ice is probably larger than shown in Figure 8, since the Holocene ice is predominantly deforming by pure shear, while the glacial ice is predominantly deforming by simple shear (Montagnat et al., 2014).

Both deformation mechanisms of the composite flow law assume basal slip to be the dominant strain producing mechanism and being accommodated by either grain boundary sliding or non-basal slip. It is therefore argued that both dislocation creep and GBS-limited creep are enhanced by a strong single maximum CPO as a strong alignment of the dominant slip system produces less strain incompatibilities at grain boundaries and/or triple junctions. Therefore, less accommodation of basal slip is required by GBS or non-basal slip or less removal of strain incompatibilities by SIBM. To what extent these two deformation mechanisms are enhanced by CPO remains the subject of further research.

The elongated aspect ratio found in sub-horizontal fine grained bands (Figure 1b) have a similar aspect ratio to grains reported by Goldsby and Kohlstedt (1997, Figure 6 therein) in the GBS-limited creep experiments. Also, similar to Goldsby and Kohlstedt (1997), aligned grain boundaries and numerous quadruple junctions were found (Figure 1b). These flattened grains, aligned grain boundaries and quadruple junctions were only found in the finest grained parts of the glacial ice, which could well indicate that these layers deform by a similar mechanism as in the GSS deformation experiments of Goldsby and Kohlstedt (1997, 2001).

5.6 Dominance of GBS-limited creep over dislocation creep

The results obtained using the original flow law parameters (Table 1) show that dislocation creep contributes more to bulk strain rate than GBS-limited creep in the Holocene ice, while in the glacial ice the dominant deformation mechanism depends on the grain size (Figure 7). The results using the modified flow law parameters (Table 2) suggest that ice deformation in the upper 2207 m of depth in the NEEM ice core is almost entirely produced by GBS-limited creep (Figure 8). However, there is evidence that significant non-basal slip is activated in the polar ice sheets (e.g. Weikusat et al., 2009b, b, 2011, 2017). Goldsby (2006) compared the results of the composite flow law using the original flow law parameters (Table 1) to the grain size and strain rate variability with depth in the basal layer of the Meserve glacier, Antarctica (Cuffey et al., 2000b). It was found that the composite flow law overestimates the contribution of GBS-limited creep in the basal part of the Meserve glacier. The in-situ temperature (256K) and the estimated shear stress (0.05 MPa) in the basal layer of the Meserve glacier are fairly similar



to the temperature and stress estimated for the glacial ice in the NEEM ice core (Figure 8c). With the modified flow law parameters for dislocation creep (Table 2), the calculated contribution of GBS-limited creep to total strain rate would be close to 100%, which is similar to the results with the NEEM ice core (Figure 8). Therefore, it is proposed that the composite flow law severely underestimates the strain rate produced by dislocation creep, as high stresses of about 0.25 MPa are required for dislocation creep to become roughly as fast as GBS-limited creep in the NEEM ice core (Figure 10a). This while the large and interlocking grains in the Holocene ice of the NEEM ice core (Figure 1a) argue against GBS as the dominant accommodating mechanism for basal slip. The results using the original flow law parameters (Table 1), where dislocation creep is the dominant deformation mechanism in the Holocene ice (Figure 7), agrees well with the ice microstructures (Figure 1a). However, in order for dislocation creep to be as fast as GBS-limited creep in the Holocene ice with the modified flow law parameters (Table 2), a strain rate increase of about an order of magnitude for dislocation creep is needed.

The deformation experiments in the GSI and GSS regime of Goldsby and Kohlstedt (1997, 2001) were performed at low temperature in order to prevent grain growth during the deformation experiments. Significant grain growth during the deformation experiments would have complicated the derivation of the flow law parameters in the GSS creep regime. Goldsby and Kohlstedt (1997) stated that “grains in deformed samples were equiaxed with straight grain boundaries; irregular grain boundaries typical of dynamical recrystallization by grain boundary migration were not observed”. However, suppressing SIBM during the deformation experiments also meant that SIBM could not remove strain incompatibilities at grain boundaries and/or triple junctions. SIBM is considered an important softening mechanism in polar ice (e.g. Duval et al., 2000; Montagnat and Duval, 2000; 2004). It is well established that SIBM is active at all depths in polar ice cores (e.g. Weikusat et al., 2009a), although the amount of SIBM varies strongly with depth (e.g. Duval and Castelnau, 1995; Kipfstuhl et al., 2009; Faria et al., 2014a). In the NEEM ice core, SIBM is probably less extensive in the finer grained glacial ice than in the coarser grained interglacial ice, which is supported by the lower grain boundary curvature in the glacial ice (Binder, 2014). It is therefore proposed that SIBM is an important softening mechanism in the NEEM ice core, while it was suppressed during the deformation experiments of Goldsby and Kohlstedt (1997, 2001). Therefore, the ice during the GSI deformation experiments of Goldsby and Kohlstedt (2001) was likely relatively hard as it was not softened by SIBM. This would have affected the flow law parameters that were derived from the results of these deformation experiments, potentially underestimating dislocation creep strain rates when using the composite flow law.

6 Conclusions

In order to study the effect of grain size and grain size variation with depth in polar ice sheets, the composite flow law of Goldsby and Kohlstedt (2001) was used with temperature and grain size data from the upper 2207 m of depth in the NEEM ice core. GSS deformation was described using a mean grain size and a grain size distribution in combination with two model end members: the micro-scale constant stress model and the micro-scale constant strain rate model. A modification of the flow



law parameters for dislocation creep (GSI) in the composite flow law showed a better fit with the experimental data obtained during the deformation experiments of Goldsby and Kohlstedt (1997, 2001).

The results using the original flow law parameter showed that dislocation creep is the dominant deformation mechanism in the Holocene ice, while GBS-limited creep and dislocation creep have roughly the same strength in the glacial ice. The results using the modified flow law parameters show that GBS-limited creep produces almost all deformation in the upper 2207 m of depth in the NEEM ice core. The difference between the model end members is relatively small with the micro-scale constant stress model predicting higher strain rates than the micro-scale constant strain rate model and using a mean grain size. A strain rate increase, mainly resulting from a reduction in grain size, is observed below 1400 m of depth for all model end members. Two depths in the glacial ice with a higher strain rate, caused by enhanced GBS-limited creep, are identified at about 1980 m and 2100 m of depth. The microstructures in the glacial ice and the rheological model indicate that the fine-grained layers in the glacial ice act as internal preferential sliding zones in the Greenland ice sheet.

At the grain size and temperature conditions of the NEEM ice core, GBS-limited creep is the dominant deformation mechanism over dislocation creep for equivalent stresses up to about 0.25 MPa. At higher stresses, which are only reached at the margins of the polar ice sheets, dislocation creep is dominant over GBS-limited creep. At low stresses of about 0.01 MPa, the composite flow law predicts a faster strain rate than Glen's flow law. However, the stress exponent of Glen's flow law is higher than the effective stress exponent for the composite flow law and therefore the strain rate increase with increasing stress is higher for Glen's flow law than for the composite flow law. At NEEM grain size and temperature conditions, Glen's flow law predicts a higher strain rate than the composite flow law at equivalent stresses higher than 0.05 MPa.

Dislocation creep with the modified flow law parameters in the composite flow law under NEEM temperatures, grain sizes and stresses is remarkably slow, both in absolute strain rate and compared to the strain rate predicted by GBS-limited creep. One possible explanation for this is that SIBM was not active during the experiments of Goldsby and Kohlstedt (1997, 2001), while SIBM is an important softening mechanism in polar ice.

Acknowledgements

This work has been carried out as part of the Helmholtz Junior Research group "The effect of deformation mechanisms for ice sheet dynamics" (VH-NG-802). The NEEM light microscope data used in this study has been made available by www.pangaea.de. The authors would like to thank Sepp Kipfstuhl and Tobias Binder for providing data and encouraging discussions. The authors would like to thank all the NEEM Community members who were involved in the preparation of the physical properties samples in the field. This work is a contribution to the NEEM ice core project which is directed and organized by the Center of Ice and Climate at the Niels Bohr Institute and US NSF, Office of Polar Programs. It is supported by funding agencies and institutions in Belgium (FNRS-CFB and FWO), Canada (NRCan/GSC), China (CAS), Denmark (FIST), France (IPEV, CNRS/INSU, CEA and ANR), Germany (AWI), Iceland (RannIs), Japan (NIPR), South Korea



(KOPRI), the Netherlands (NOW/ALW), Sweden (VR), Switzerland (SNF), the United Kingdom (NERC) and the USA (US NSF, Office of Polar Programs).

References

- Alley, R. B.: Flow-law hypothesis for ice-sheet modelling. *Journal of Glaciology*, 38, 245-256, 1992.
- 5 Alley, R. B., Clark, P. U., Huybrechts, P., and Joughin, I.: Ice-Sheet and Sea-Level changes. *Science*, 310, 456-460, doi:10.1126/science.1114613, 2005.
- Azuma, N.: A flow law for anisotropic ice and its application to ice sheets. *Earth and Planetary Science Letters*, 128, 601-614, doi:10.1016/0012-821X(94)90173-2, 1994.
- Baker, R. W.: Textural and Crystal-Fabric Anisotropies and the Flow of Ice Masses. *Science, New Series*, 211, 1043-1044,
10 1981.
- Barnes, P., Tabor, D., and Walker, J. C. F.: The friction and creep of polycrystalline ice. *Proceedings Royal Society London A*, 324, 127-155, 1971.
- Binder, T., Weikusat, I., Freitag, J., Garbe, C. S., Wagenbach, D., and Kipfstuhl, S.: Microstructure through an ice sheet. *Materials Science Forum*, 753, 481-484, doi:10.4028/www.scientific.net/MSF.753.481, 2013.
- 15 Binder, T.: Measurements of grain boundary networks in deep polar ice cores – A digital image processing approach. PhD thesis, University of Heidelberg, Germany, doi:10.11588/heidok.00016891, 2014, <http://archiv.ub.uni-heidelberg.de/volltextserver/16891/>.
- Bintanja, R.: *Glacier Science and environmental change* (eds. by P. G. Knight). pp. 174-176. Blackwell, Oxford, 2009.
- Bons, P. D., and Jessell, M. W.: Micro-shear zones in experimentally deformed octachloropropane. *Journal of Structural
20 Geology*, 21, 323-334, doi:10.1016/S0191-8141(98)90116-X, 1999.
- Bons, P. D., Kleiner, T., Llorens, M.-G., Prior, D. J., Sachau, T., Weikusat, I., and Jansen, D.: Greenland Ice Sheet: Higher Nonlinearity of ice Flow Significantly Reduces Estimated Basal Motion. *Geophysical Research Letters*, 45, 1-7, doi:10.1029/2018GL078356, 2018.
- Budd, W. F., and Jacka, T. H.: A review of ice rheology for ice sheet modelling. *Cold Regions Science and Technology*, 16,
25 107-144, doi:10.1016/0165-232X(89)90014-1, 1989.
- Church, J. et al.: “Climate Change 2013: The Physical Science Basis. Contribution of Working Group I to the Fifth Assessment Report of the Intergovernmental Panel on Climate Change”. Ed. by T. Stocker et al. Cambridge University Press, Cambridge, United Kingdom and New York, NY, USA. Chap. Sea Level Change (cit. on p. 1), 2013.
- Cuffey, K. M., Conway, H., Gades, A., Hallet, B., Raymond, C. F., and Whitlow, S.: Deformation properties of subfreezing
30 glacier ice: Role of crystal size, chemical impurities, and rock particles inferred from in situ measurements. *Journal of Geophysical Research*, 105, 27895-27915, doi:10.1029/2001JB900014, 2000b.



- Cuffey, K. M., Thorsteinsson, T., and Waddington, E. D.: A renewed argument for crystal size control of ice sheet strain rates. *Journal of Geophysical Research*, 105, 27889-27894, doi:10.1029/2000JB900270, 2000a.
- Dahl-Jensen, D.: Two-dimensional thermo-mechanical modelling of flow and depth-age profiles near the ice divide in central Greenland. *Annals of Glaciology*, 12, 31-36, 1989a.
- 5 Dahl-Jensen, D.: Steady Thermomechanical flow along two-dimensional flow lines in large grounded ice sheets. *Journal of Geophysical research*, 94, 10355-10362, doi:10.1029/JB094iB08p10355, 1989b.
- Dahl-Jensen, D., and Gundestrup, N. S.: Constitutive properties of ice at Dye 3. Greenland, *The Physical Basis of Ice Sheet Modelling*, 170, 31-40, 1987.
- Dansgaard, W., and Johnsen, S. J.: A flow model and a time scale for the ice core from camp century, Greenland. *Journal of*
10 *Glaciology*, 8, 215-223, doi:10.3189/S0022143000031208, 1969.
- De La Chapelle, S., Castelnau, O., Lipenkov, V., and Duval, P.: Dynamic recrystallization and texture development in ice as revealed by the study of deep ice cores in Antarctica and Greenland. *Journal of Geophysical Research*, 103, 5091-5105, 1998.
- De La Chapelle, S., Milsch, H., Castelnau, O., and Duval, P.: Compressive creep of ice containing a liquid intergranular phase: rate-controlling processes in the dislocation creep regime. *Geophysical Research Letter*, 26, 251-254,
15 doi:10.1029/1998GL900289, 1999.
- Drury, M. R., Avé Lallemant, H. G., Pennock, G. M., and Palasse, L. N.: Crystal preferred orientation in peridotite ultramylonites deformed by grain size sensitive creep, Étang de Lers, Pyrenees, France. *Journal Structural Geology*, 33, 1776-1789, doi:10.1016/j.jsg.2011.10.002, 2011.
- Durham, W. B., Prieto-Ballesteros, O., Goldsby, D. L., and Kargel, J. S.: Rheological and Thermal Properties of Icy Materials.
20 *Space Science Reviews*, 153, 273-298, doi:10.1007/s111214-009-9619-1, 2010.
- Durham, W. B., and Stern, L. A.: Rheological Properties of Water Ice – Applications to satellites of the Outer Planets. *Annual Review of Earth and Planetary Science*, 29, 295-330, 2001.
- Duval, P., Arnaud, L., Brissaud, O., Montagnat, M., and De La Chapelle, S.: Deformation and recrystallization processes of ice from polar ice sheets. *Annals of Glaciology*, 30, 83-87, doi:10.3189/172756400781820688, 2000.
- 25 Duval, P., Ashby, M. F., and Anderman, I.: Rate-controlling processes in the creep of polycrystalline ice. *Journal of Physical Chemistry*, 87, 4066-4074, doi:10.1021/j100244a014, 1983.
- Duval, P., and Castelnau, O.: Dynamic recrystallization of ice in polar ice sheets. *Journal de Physique III*, 05, 197-205, doi:10.1051/jp4:1995317, 1995.
- Eichler, J., Kleitz, I., Bayer-Giraldi, M., Jansen, D., Kipfstuhl, S., Shigeyama, W., Weikusat, C., and Weikusat, I.: Location
30 and distribution of micro-inclusions in the EDML and NEEM ice cores using optical microscopy and in situ Raman spectroscopy. *The Cryosphere*, 11, 1075-1090, doi:10.5194/tc-11-1075-2017, 2017.
- Eichler, J., Weikusat, I., and Kipfstuhl, S.: Orientation-tensor eigenvalues along the NEEM ice core. *PANGAEA*, <https://doi.org/10.1594/Pangaea.838059>, 2013.



- Faria, S. H., Freitag, J., and Kipfstuhl, S.: Polar ice structure and the integrity of ice-core paleoclimate records. *Quaternary Science Reviews*, 29, 1-2, 338-351, doi:10.1016/j.quascirev.2009.10.016, 2010.
- Faria, S. H., Weikusat, I., and Azuma, N.: The microstructure of polar ice. Part II: State of the art. *Journal of Structural Geology*, 61, 21-49, doi:10.1016/j.jsg.2013.11.003, 2014a.
- 5 Faria, S. H., Weikusat, I., and Azuma, N.: The microstructure of polar ice. Part I: Highlights from ice core research. *Journal of Structural Geology*, 61, 2-20, doi:10.1016/j.jsg.2013.09.010, 2014b.
- Freeman, B., and Ferguson, C.: Deformation mechanism maps and micromechanics of rocks with distributed grain sizes. *Journal of Geophysical Research*, 91, 3849-3860, doi:10.1029/JB091iB03p03849, 1986.
- Fisher, D. A., and Koerner, R. M.: On the special rheological properties of ancient microparticle-laden northern hemisphere
10 ice as derived from bore-hole and core measurements. *Journal of Glaciology*, 32, 501-510, 1986.
- Fitzpatrick, J. J., Voigt, D. E., Fegyveresi, J. M., Stevens, N. T., Spencer, M. K., Cole-dai, J., Alley, R. B., Jardine, G. E., Cravens, E. D., Wilen, L. A., Fudge, T. J., and McConnell, J. R.: Physical properties of the WAIS Divide ice core. *Journal of Glaciology*, 60, 1181-1198, doi:10.3189/2013JoG14j100, 2014.
- Gillet-Chaulet, F., Hindmarsh, R. C. A., Corr, H. F. J., King, E. C., and Jenkins, A.: In-situ quantification of ice rheology and
15 direct measurement of the Raymond Effect at Summit, Greenland using a phase-sensitive radar. *Geophysical Research Letter*, 38, 381-6, doi:10.1029/2011GL049843, 2011.
- Glen, J. W.: Experiments on the deformation of ice. *Journal of Glaciology*, 2, 111-114, 1952.
- Glen, J. W.: The creep of polycrystalline ice. *Proceedings of the Royal Society A: Mathematical, Physical and Engineering Sciences*, 228, 519-538, doi:10.1098/rspa.1955.0066, 1955.
- 20 Goldsby, D. L., and Kohlstedt, D. L.: Grain boundary sliding in fine grained ice I. *Scripta Materialia*, 37, 9, 1399-1406, 1997.
- Goldsby, D. L., and Kohlstedt, D. L.: Superplastic deformation of ice: Experimental observations. *Journal of Geophysical Research*, 106, B6, 11017-11030, doi:10.1029/2000JB900336, 2001.
- Goldsby, D. L., and Kohlstedt, D. L.: Reply to comment by P. Duval and M. Montagnat on "Superplastic deformation of ice: Experimental observations". *Journal of Geophysical Research*, 107, B11, 1-5, doi:10.1029/2002JB001842, 2002.
- 25 Goldsby, D. L.: Superplastic Flow of Ice Relevant to Glacier and Ice-Sheet Mechanics, *Glacier Science and Environmental Change*, edited by: Knight, P. G., Blackwell Publishing, Malden, MA, USA, 308-314, doi:10.1002/9780470750636.ch60, 2006.
- Gow, A. J., Meese, D. A., Alley, R. B., Fitzpatrick, J. J., Anandkrishnan, S., Woods, G. A., and Elder, B. C.: Physical and structural properties of the Greenland Ice Sheet Project 2 ice core: A review. *Journal of Geophysical Research*, 102, 26559-
30 26575, doi:10.1029/97JC00165, 1997.
- Greve, R., and Blatter, H.: *Dynamics of ice sheets and glaciers*. Springer Berlin/Heidelberg, 2009.
- Hansen, L. N., Zimmerman, M. E., and Kohlstedt, D. L.: Grain boundary sliding in San Carlos olivine: Flow law parameters and crystallographic-preferred orientation. *Journal of Geophysical Research: Solid Earth*, 116, 1-16, doi:10.1029/2011JB008220, 2011.



- Hansen, L. N., Zimmerman, M. E., and Kohlstedt, D. L.: The influence of microstructure on deformation of olivine in the grain-boundary sliding regime. *Journal of Geophysical Research: Solid Earth*, 117, 1-17, doi:10.1029/2012JB009305, 2012.
- Heilbronner, R., and Bruhn, D.: The influence of three-dimensional grain size distributions on the rheology of polyphaser rocks. *Journal of structural Geology*, 20, 695-705, doi:10.1016/S0191-8141(98)00010-8, 1998.
- 5 Herwegh, M., Bresser, J. H. P., and Ter Heege, J. H.: Combining natural microstructures with composite flow laws: an improved approach for the extrapolation of lab data to nature. *Journal of Structural Geology*, 27, 503-521, doi:10.1016/j.jsg.2004.10.010, 2005.
- Hutter, K.: *Theoretical glaciology; material science of ice and the mechanics of glaciers and ice sheets*. Reidel Publishing Co., Dordrecht, Terra Scientific Publishing Co, Tokyo, 1983.
- 10 Huybrechts, P.: Ice sheet modelling, *Encyclopedia of the Antarctic* (ed. by Riffenburgh, B.), pp 514-417. Routledge. New York and London, 2007.
- IPCC.: *Climate change 2014: Synthesis report. contribution of working groups i, ii, iii to the fifth assessment report of the intergovernmental panel on climate change*, IPCC, Geneva, Switzerland, 151, 2014.
- Jansen, D., Llorens, M.-G., Westhoff, J., Steinbach, F., Kipfstuhl, S., Bons, P. D., Grier, A., and Weikusat, I.: Small-scale
15 disturbances in the stratigraphy of the NEEM ice core: observations and numerical simulations. *The Cryosphere*, 10, 359-370, doi:10.5194/tc-10-359-2016, 2016.
- Kipfstuhl, S.: Large area scan microscope images from the NEEM ice core. Alfred Wegener Institute, Helmholtz Centre for Polar and Marine Research, Bremerhaven, Pangaea, <https://doi.pangaea.de/10.1594/PANGAEA.743296> (unpublished dataset), 2010.
- 20 Kipfstuhl, S., Faria, S. H., Azuma, N., Freitag, J., Hamann, I., Kaufmann, P., Miller, H., Weiler, and K., Wilhelms, F.: Evidence of dynamic recrystallization in polar firn. *Journal of Geophysical Research*, 114, 1-10, doi:10.1029/2008JB005583, 2009.
- Kipfstuhl, S., Hamann, I., Lambrecht, A., Freitag, J., Faria, S. H., Grigoriev, D., and Azuma, N.: Microstructure mapping: a new method for imaging deformation induced microstructural features of ice on the grain scale, *Journal of Glaciology*, 52, 398-406, doi:10.3189/172756506781828647, 2006.
- 25 Kirby, S., Durham, W., Beeman, M., Heard, H., and Daley, M.: Inelastic properties of ice I_h at low temperatures and high pressures. *Journal de Physique Colloques*, 48, 227-232, doi:10.1051/jphyscol:1987131, 1987.
- Krischke, A., Oechsner, U., and Kipfstuhl, S.: Rapid Microstructure Analysis of Polar Ice Cores. *Optik & Photonik*, 10, 32-35, doi:10.1002/opph.201500016, 2015.
- Marshall, S. J.: Modelling glacier response to climate change. In Knight, P. G., editor, *Glacier Science and Environmental*
30 *Change*. 163-173. Blackwell Publishing, 2006.
- Mellor, M., and Testa, R.: Creep of ice under low stress. *Journal of Glaciology*, 8, 147-152, 1969a.
- Mellor, M., and Testa, R.: Effect of temperature on the creep of ice. *Journal of Glaciology*, 8, 131-145, 1969b.



- Montagnat, M., Azuma, N., Dahl-Jensen, D., Eichler, J., Fujita, S., Gillet-Chaulet, F., Kipfstuhl, S., Samyn, D., Svenson, A., and Weikusat, I.: Fabric along the NEEM ice core, Greenland, and its comparison with GRIP and NGRIP ice core. *The Cryosphere*, 8, 1129-1138, doi:10.5194/tc-8-1129-2014, 2014.
- Montagnat, M., and Duval, P.: Rate controlling processes in the creep of polar ice, influence of grain boundary migration associated with recrystallization. *Earth and Planetary Science Letter*, 183, 179-186, doi:10.1016/S0012-821X(00)00262-4, 2000.
- Montagnat, M., and Duval, P.: Dislocations in ice and Deformation Mechanisms: from Single Crystals to Polar Ice. *Defect and Diffusion Forum*, 229, 43-54, 2004.
- Morgan, V. I.: High-Temperature ice creep tests. *Cold Regions Science and Technology*, 19, 295-300, 1991.
- NEEM community members.: Eemian interglacial reconstructed from a Greenland folded ice core. *Nature*, 493, 489-494, doi:10.1038/nature11789, 2013.
- Obbard, R., Baker, I., and Sieg, S.: Using electron backscatter diffraction patterns to examine recrystallization in polar ice sheets. *Journal of Glaciology*, 52, 546-557, 2006.
- Paterson, W. S. B.: Why ice-age ice is sometimes “soft”. *Cold Regions Science and Technology*, 20, 75-98, doi:10.1016/0165-232X(91)90058-O, 1991.
- Paterson, M. S., and Olgaard, D. L.: Rock deformation tests to large shear strains in torsion. *Journal of Structural Geology*, 22, 1341-1358, doi:10.1016/S0191-8141(00)00042-0, 2000.
- Paterson, W. S. B.: *The physics of glaciers*, Third edition. Oxford, Elsevier, 1994.
- Peltier, W. R., Goldsby, D. L., Kohlstedt, D. L., and Tarasov, L.: Ice-age ice-sheet rheology: constraints from the Last Glacial Maximum form of the Laurentide ice sheet. *Annals of Glaciology*, 30, 163-176, doi:10.3189/172756400781820859, 2000.
- Petrenko, V. F., and Withworth, R. W.: *Physics of ice*. Oxford University Press, Oxford, 1999.
- Piazolo, S., Montagnat, M., Grennerat, F., Moulinec, H., and Wheeler, J.: Effect of local stress heterogeneities on dislocation fields: Examples from transient creep in polycrystalline ice. *Acta Materialia*, 90, 303-309, doi:10.1016/j.actamat.2015.02.046, 2015.
- Pimienta, P., and Duval, P.: Rate controlling processes in the creep of polar glacier ice. *Journal de Physique Colloques*, 48, 243-248, doi:10.1051/jphyscol:1987134, 1987.
- Rasmussen, S. O., Abbott, P. M., Blunier, T., Bourne, A. J., Brook, E., Buchardt, S. L., Buizert, C., Chappellaz, J., Clausen, H. B., Cook, E., Dahl-Jensen, D., Davies, S. M., Guillevic, M., Kipfstuhl, S., Laepple, T., Seierstad, I. K., Severinghaus, J. P., Steffensen, J. P., Stowasser, C., Svensson, A., Vallelonga, P., Vinther, B. M., Wilhelms, F., and Winstrup, M.: A first chronology for the North Greenland Eemian Ice Drilling (NEEM) ice core. *Climate of the Past*, 9, 2713-2730, doi:10.5194/cp-9-2713-2013, 2013.
- Raymond, C. F.: Deformation in the vicinity of ice divides. *Journal of Glaciology*, 29, 357-373, 1983.
- Rutter, E. H., Casey, M., and Burlini, L.: Preferred crystallographic orientation development during the plastic and superplastic flow of calcite rocks. *Journal of Structural Geology*, 16, 1431-1446, doi:10.1016/0191-8141(94)90007-8, 1994.



- Schmid, S. M., Pazonno, R., and Bauer, S.: Simple shear experiments on calcite rocks: Rheology and microfabric, *Journal of Structural Geology*, 9, 747-778, doi:10.1016/0191-8141(87)90157-X, 1987.
- Schultson, E. M., and Duval, P.: *Creep and Fracture of Ice*. Cambridge University Press, 2009.
- Sergienko, O. V., Creyts, T. T., and Hindmarsh, R. C. A.: Similarity of organized patterns in driving and basal stresses of Antarctic and Greenland ice sheets beneath extensive areas of basal sliding. *Geophysical Research Letter*, 41, 3925-3932, doi:10.1002/2014GL059976, 2014.
- Sheldon, S. G., Steffensen, J. P., Hansen, S. B., Popp, T. J., and Johnson, S. J.: The investigation and experience of using ESTISOL™ 240 and COASOL™ for ice-core drilling. *Annals of Glaciology*, 55, 219-232, doi:10.3189/2014AoG68A036, 2014.
- 10 Ter Heege, J. H., De Bresser, J. H. P., and Spiers, C. J.: Composite flow laws for crystalline materials with log normally distributed grain size: theory and application to olivine. *Journal Structural Geology*, 26, 1693-1705, doi:10.1016/j.jsg.2004.01.008, 2004.
- Thoma, M., Grosfeld, K., Mayer, C., and Pattyn, F.: Interaction between ice sheet dynamics and subglacial lake circulation: a coupled modelling approach. *The Cryosphere*, 4, 1-12. doi:10.5194/tc-4-1-2010, 2010.
- 15 Thorsteinsson, T., Waddington, E.D., Taylor, K. C., Alley, R. B., and Blankenship, D. D.: Strain-rate enhancement at Dye 3, Greenland. *Journal of Glaciology*, 45, 338-345, doi:10.3189/002214399793377185, 1999.
- Treverrow, A., Budd, W. F., Jacka, T. H., and Warner, R. C.: The tertiary creep of polycrystalline ice: experimental evidence for stress-dependent levels of strain-rate enhancement. *Journal of Glaciology*, 58, 301-314, doi:10.3189/2012JoG11J149, 2012.
- 20 Vaughan, D. G., and Arthern, R.: Why is it hard to predict the future of ice sheets? *Science*, 315, 1503-1504, doi:10.1126/science.1141111, 2007.
- Waddington, E. D.: Life, death and afterlife of the extrusion flow theory. *Journal of Glaciology*, 56, 973-996, doi:10.3189/002214311796406022, 2010.
- Weertman, J.: Creep deformation of ice. *Annual Review of Earth and Planetary Sciences*, 11, 215-240, 1983.
- 25 Weikusat, I., Kipfstuhl, S., Azuma, N., Faria, S. H., and Miyamoto, A.: Deformation microstructures in an Antarctic ice core (EDML) and in experimentally deformed artificial ice. *Physics of Ice Core Records II*, 68, 115-123, 2009b.
- Weikusat, I., Kipfstuhl, S., Faria, S. H., Azuma, N., and Miyamoto, A.: Subgrain boundaries and related microstructural features in EDML (Antarctica) deep ice core. *Journal of Glaciology*, 55, 461-472, 2009a.
- Weikusat, I., Kuiper, E. N., Pennock, G. M., Kipfstuhl, S., and Drury, M. R.: EBSD analysis of subgrain boundaries and dislocation slip systems in Antarctic and Greenland ice. *Solid Earth*, 8, 883-898, doi:10.5194/se-8-883-2017, 2017.
- 30 Weikusat, I., Miyamoto, A., Faria, S. H., Kipfstuhl, S., Azuma, N., and Hondoh, T.: Subgrain boundaries in Antarctic ice quantified by X-ray Laue diffraction. *Journal of Glaciology*, 57, 85-94, doi:10.3189/002214311795306628, 2011.



Wolovick, M. J., and Creyts, T. T.: Overturned folds in ice sheets: Insight from a kinematic model of travelling sticky patches and comparisons with observations. *Journal of Geophysical Research: Earth Surface*, 121, 1065-1083, doi:10.1002/2015JF003698, 2016.

5 Zhang, Y., Hobbs, B. E., and Jessell, M. W.: The effect of grain-boundary sliding on fabric development in polycrystalline aggregates. *Journal of Structural Geology*, 16, 1315-1325, doi:10.1016/0191-8141(94)90072-8, 1994.

Zwally, H. J., Abdalati, W., Herring, T., Larson, K., Saba, J., and Steffen, S.: Surface Melt-Induced Acceleration of Greenland Ice-Sheet Flow. *Science*, 297, 218-223, doi:10.1126/science.1072708, 2002.

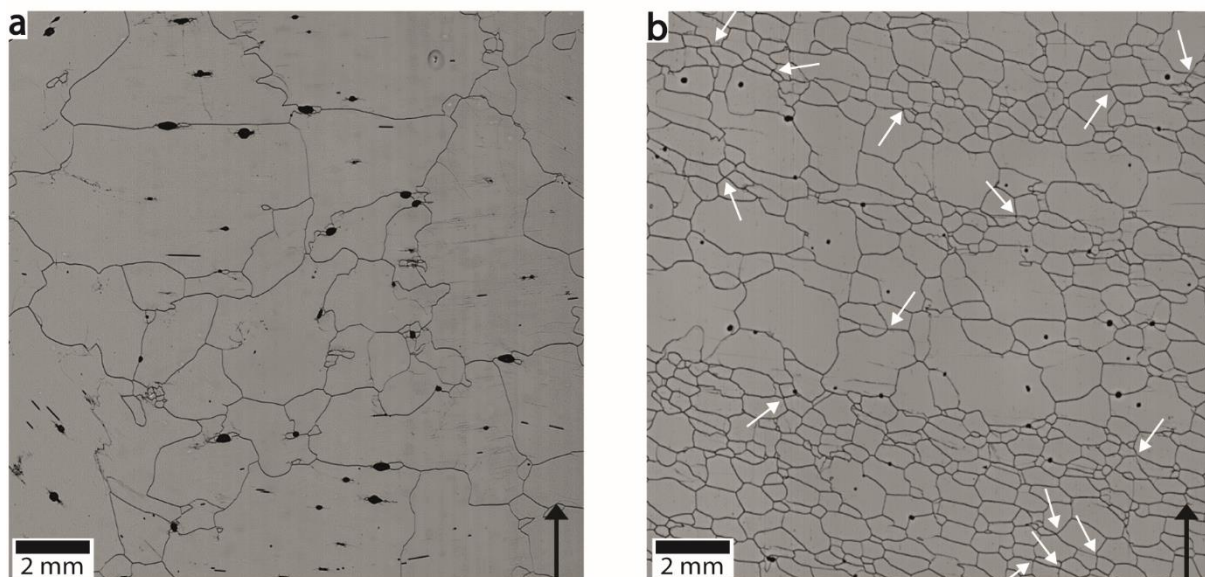


Figure 1: Reflected LM images of ice core sections at (a) 921 m of depth in the Holocene ice and (b) of 1977 m depth in the glacial ice of the NEEM ice core. The black arrows indicate the top of the ice core. The Holocene ice core section contains relatively coarse grains with an irregular grain boundary network. The glacial ice core section contains layers with coarse and relatively fine grains that are distributed in sub-horizontal bands. The fine grained sub-horizontal bands have many aligned grain boundaries and quadruple junctions which are indicated by white arrows. Images taken from Kipfstuhl (2010) (doi:10.1594/PANGAEA.743296).

5

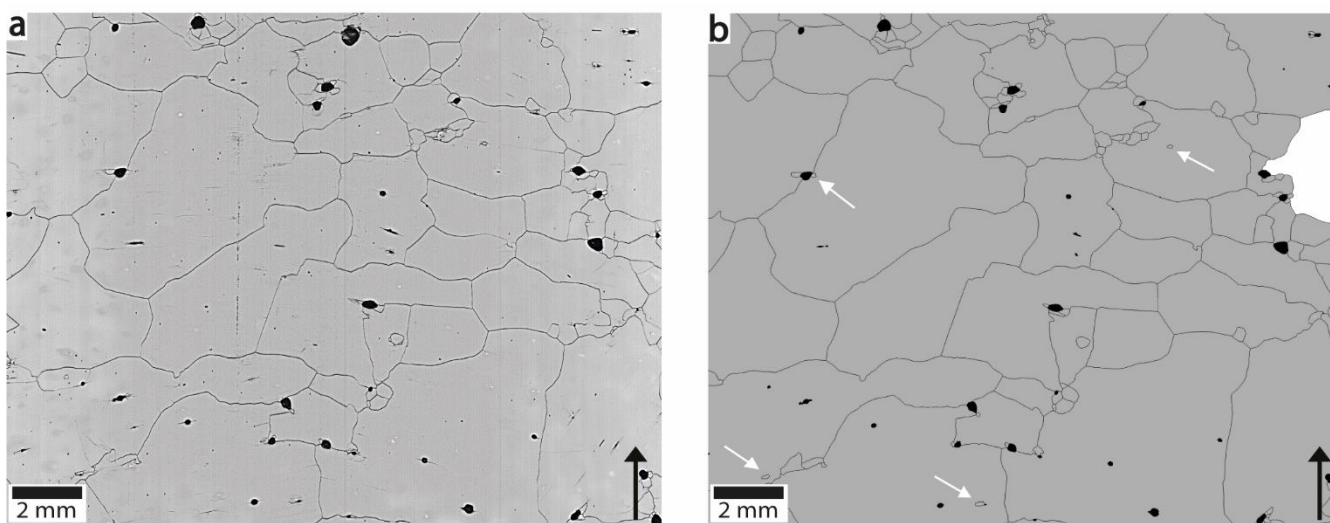


Figure 2: Reflected LM image (left) and the segmented image (right) of an ice core section at 756 m depth. The black arrows indicate the top of the ice core. White arrows indicate examples of artifacts with a diameter < 0.3 mm that were not included in the grain size data. The white grain in the upper right corner of the segmented image was excluded from the grain size data because the grain boundary was interrupted by the edge of the sample. Images taken from Kipfstuhl (2010) (doi:10.1594/PANGAEA.743296) and Binder et al. (2013).

10

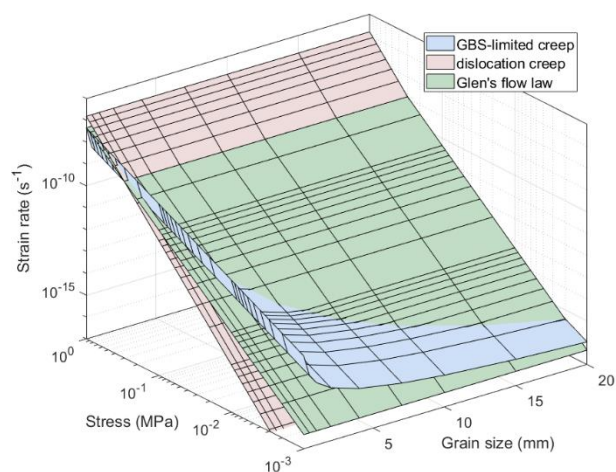


Figure 3: The effect of grain size and stress on strain rate plotted for Glen's flow, the dislocation creep mechanism and GBS-limited creep of the composite flow law at a constant temperature of 243K using the flow law parameters in Table 1.

5

Table 1: Parameters for the simplified composite flow law and Glen's flow law relating grain size, temperature and stress to strain rate (Equation 3) taken from Goldsby and Kohlstedt (2001) and Glen's flow law (Paterson, 1994).

Creep regime	A (units)	n	Q (kJ mol ⁻¹)	p
Dislocation creep (T<258K)	1.2 10 ⁶ MPa ^{-4.0} s ⁻¹ *	4.0	60	0
GBS-limited creep (T<255K)	3.9 10 ⁻³ MPa ^{-1.8} m ^{1.4} s ⁻¹	1.8	49	1.4
Glen's flow law (T<263K)	3.61 10 ⁵ MPa ^{-3.0} s ⁻¹	3.0	60	0

15 *This value of A was updated from the original value (Goldsby, 2006).

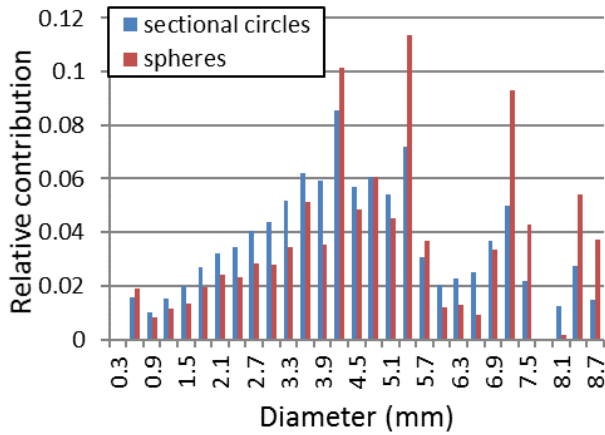
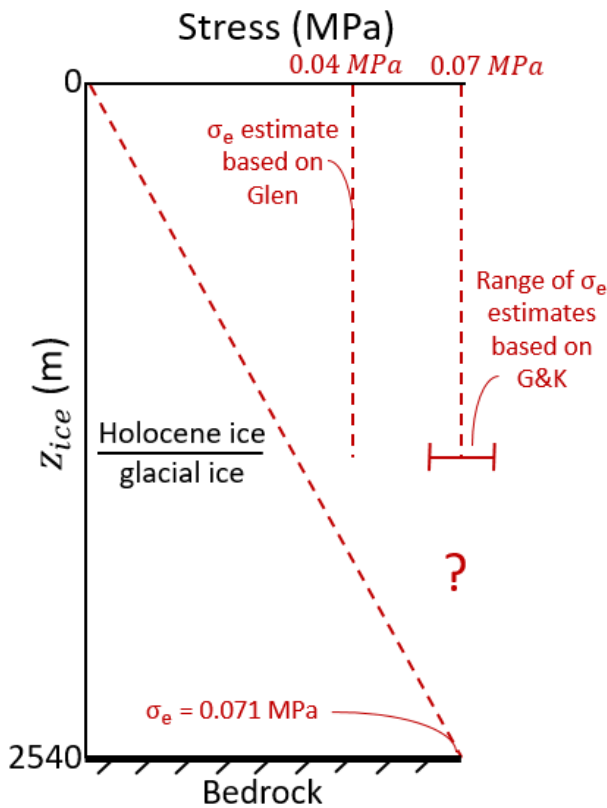
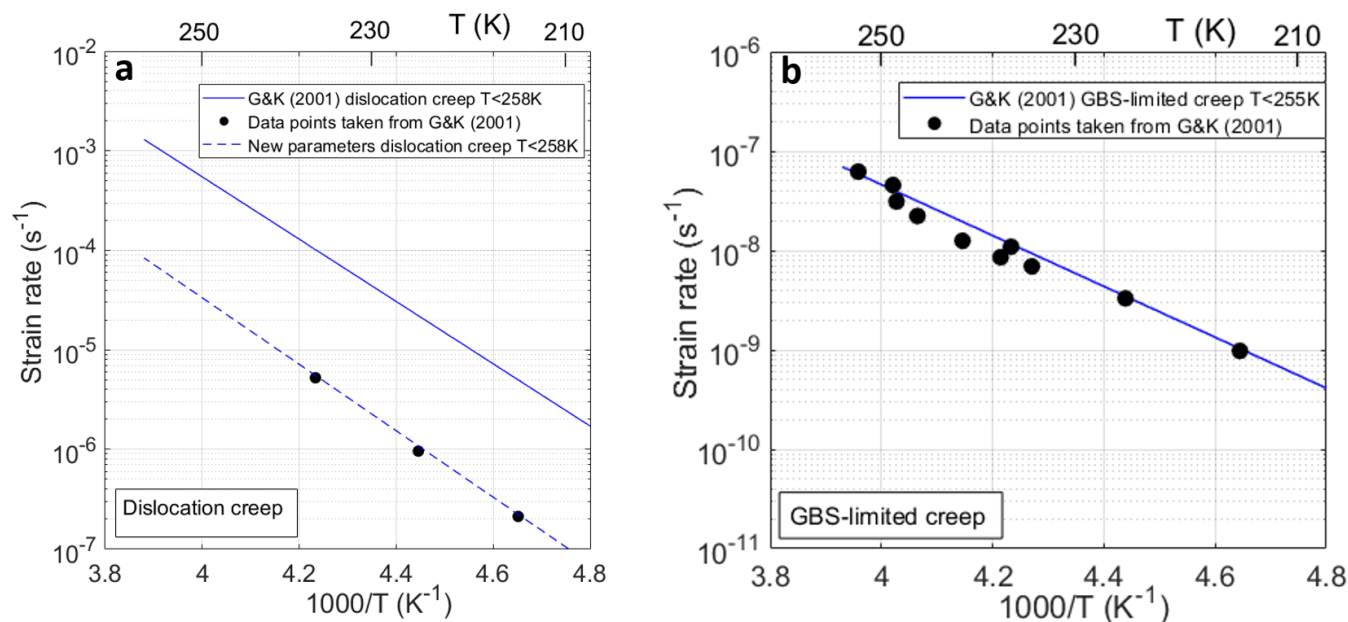


Figure 4: Relative contribution of each grain size class to the bulk volume of an ice core section at 921 m depth calculated for sectional circles (blue) and spherical grains (red) using the method of Heilbronner and Bruhn (1988).



5 Figure 5: The equivalent shear stress (σ_e) with depth calculated using the shallow ice approximation (Equation 9) and the range of the estimated longitudinal stress based on the modified parameters of the composite flow law (G&K) of Table 2 and the best estimate for Glen's flow law constrained by the annual layer thinning in the Holocene ice of the NEEM ice core. There are no constraints on the annual layer thinning in the glacial and Eemian ice, which is indicated by the question mark.



5 **Figure 6:** Arrhenius plot showing (a) the dislocation creep mechanism and (b) the GBS-limited creep mechanism below their temperature thresholds of 258K and 255K, respectively. A stress of 6.3 MPa was used to calculate the strain rates in (a) and a stress of 0.53 MPa and a uniform grain size of 73 μm was used for (b). The black dots are the experimental data points taken from Goldsby and Kohlstedt (2001). The solid lines represent the calculated strain rate using the original flow law parameters (Table 1). The dotted line is the calculated strain rates using the modified flow law parameters (Table 2).

Table 2: Modified flow law parameters for the composite flow law as derived from Figure 6.

Creep regime	A (units)	n	Q (kJ mol ⁻¹)	p
Dislocation creep (T < 262K)	$5.0 \cdot 10^5 \text{ MPa}^{-4.0} \text{ s}^{-1}$	4.0	64	0 ¹⁰
GBS-accommodated basal slip (T < 262K)	$3.9 \cdot 10^{-3} \text{ MPa}^{-1.8} \text{ m}^{1.4} \text{ s}^{-1}$	1.8	49	1.4

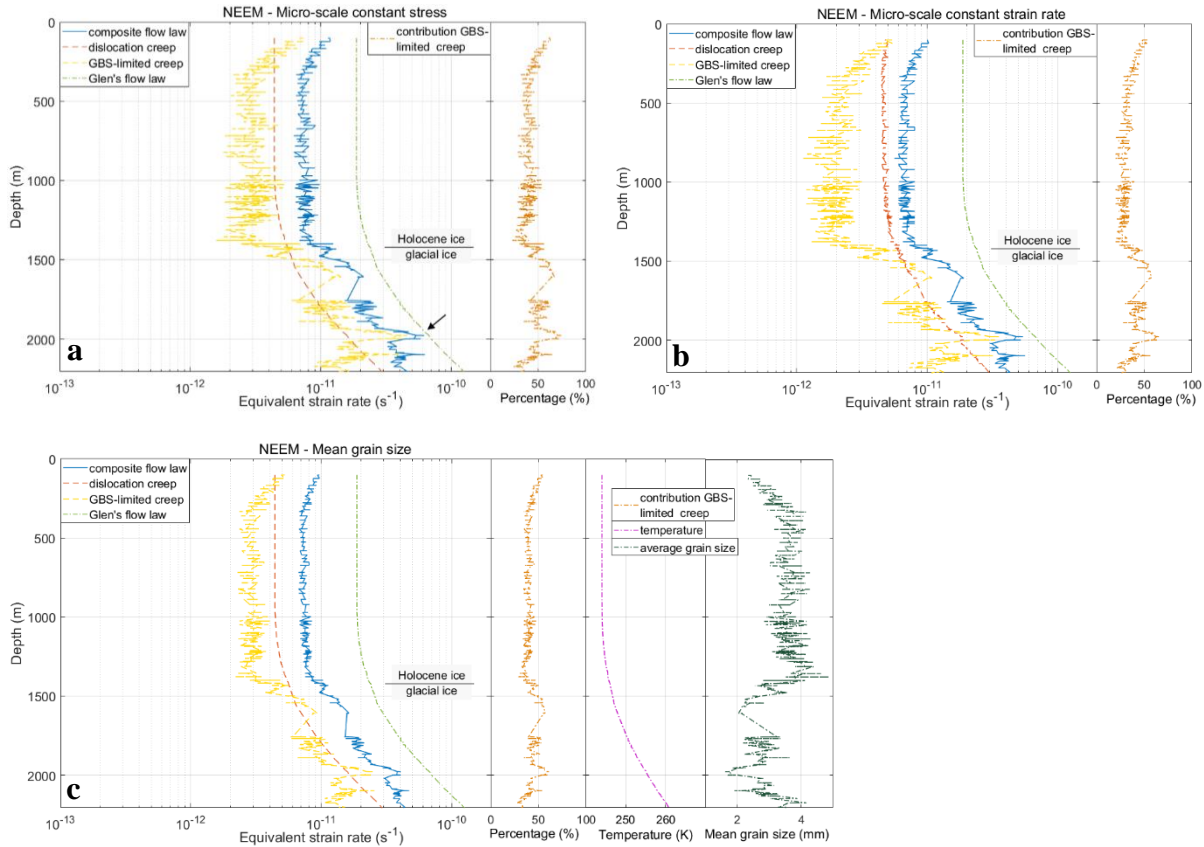
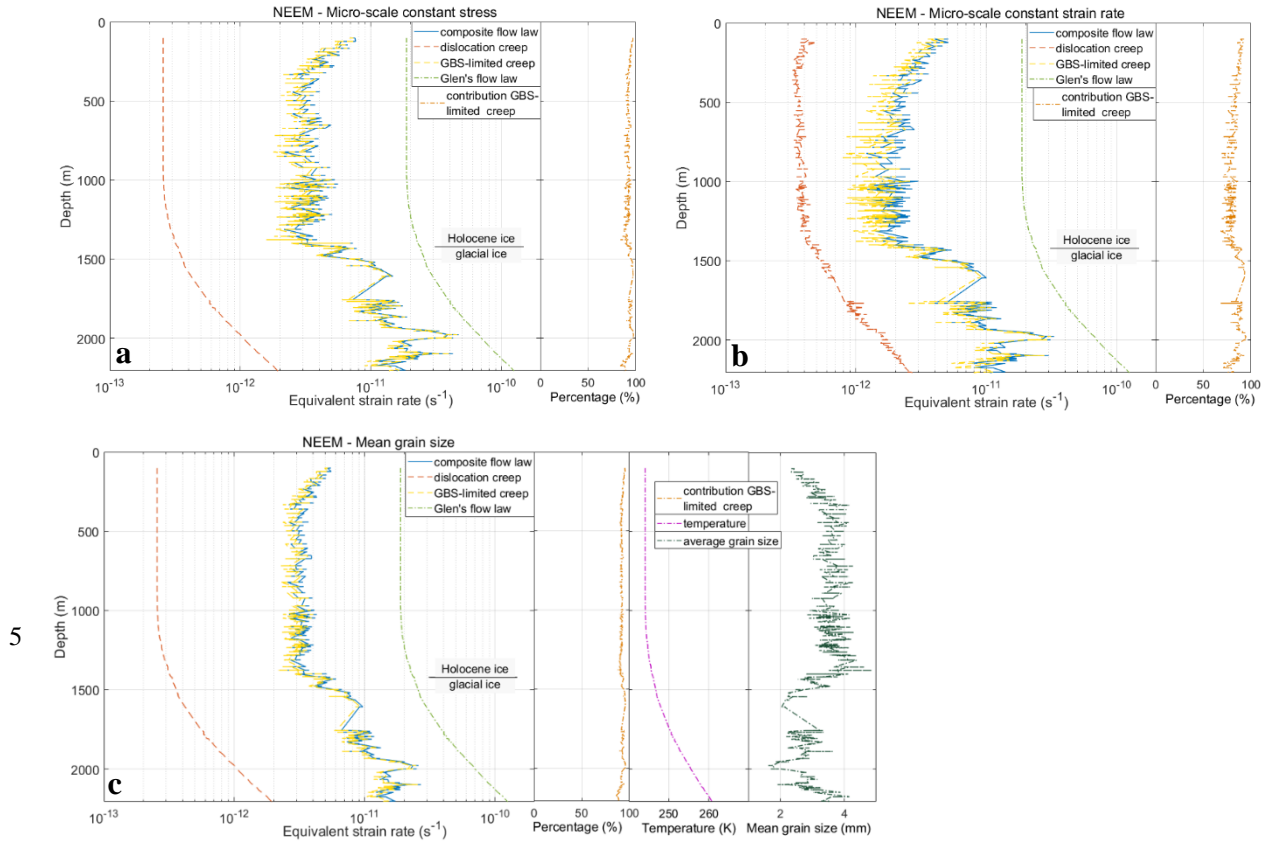


Figure 7: (a) Results for the Holocene and glacial ice for Glen's flow law (light green, same in a, b, c) and the composite flow law (blue) using the flow law parameters in Table 1, which consist of dislocation creep (red) and GBS-limited creep (yellow), using (a) the micro-scale constant stress model with the grain size distribution with the arrow indicating the depth at which Glen's flow law and the composite flow law have a similar strength, (b) the micro-scale constant strain rate model with the grain size distribution and (c) the composite flow law with the average grain size data. To show the influence of temperature and average grain size on calculated strain rates, these input parameters are added next to (c). The contribution of GBS-limited creep to bulk strain rate for all three model end members is shown. The temperature profile is used in all three figures (a, b, c), while the average grain size profile was only used for calculating the results shown in (c). A constant effective stress of 0.07 MPa was used for all figures.

10

15



10 **Figure 8:** (a) Results for the Holocene and glacial ice for Glen's flow law (light green, same in a, b, c) and the composite flow law
 (blue) using the flow law parameters in Table 2, which consist of dislocation creep (red) and GBS-limited creep (yellow), using (a)
 the micro-scale constant stress model with the grain size distribution, (b) the micro-scale constant strain rate model with the grain
 size distribution and (c) the composite flow law with the average grain size data. To show the influence of temperature and average
 grain size on calculated strain rates, these input parameters are added next to (c). The contribution of GBS-limited creep to bulk
 15 strain rate for all three model end members is shown. The temperature profile is used in all three figures (a, b, c), while the average
 grain size profile was only used for calculating the results shown in (c). A constant effective stress of 0.07 MPa was used for all
 figures.

20

25

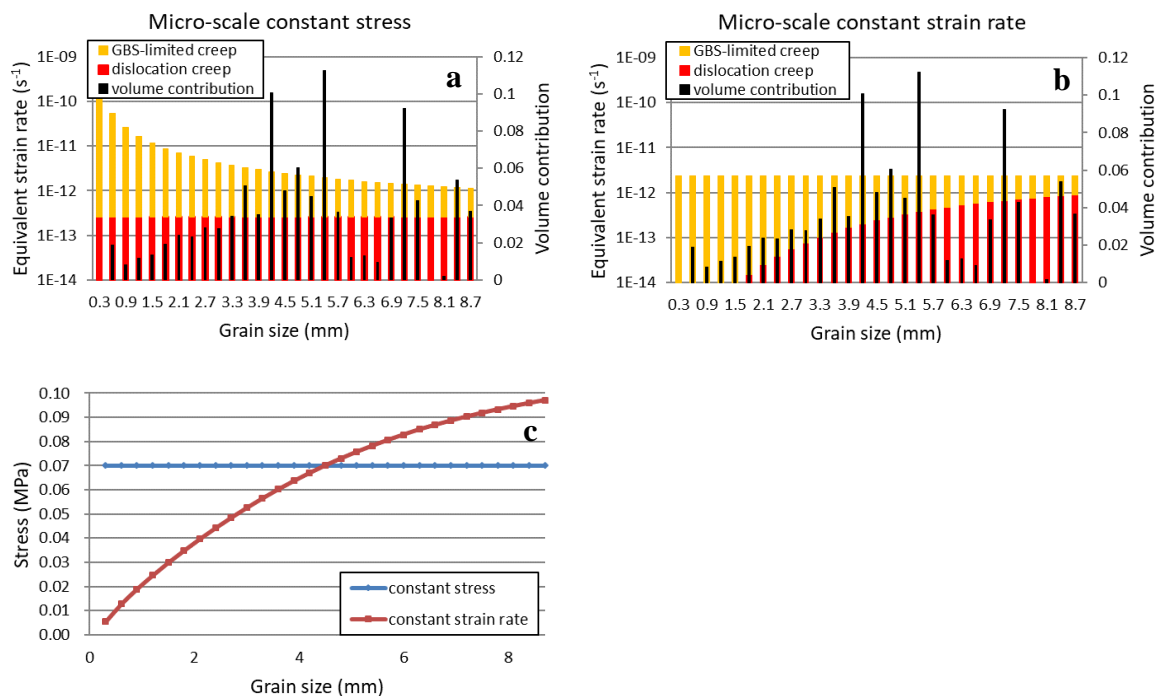


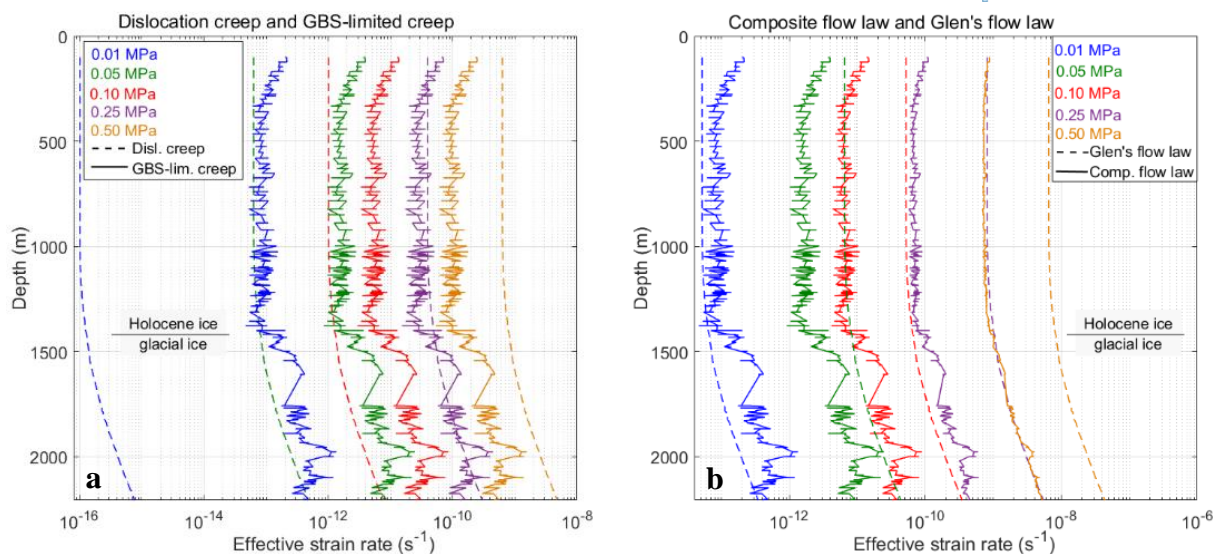
Figure 9: Grain size class versus log strain rate for an ice core section at 921 m depth for (a) the micro-scale constant stress model, (b) the micro-scale constant strain rate model and (c) the stress supported by each grain size class of the grain size distribution. The results were calculated using the flow law parameters in Table 2. The bulk strain rate for this ice core section using the micro-scale constant stress and micro-scale constant strain rate model following Equations (5) to (8) is $4.1 \cdot 10^{-12} \text{ s}^{-1}$ and $2.4 \cdot 10^{-12} \text{ s}^{-1}$, respectively.

5

10

15

20



5 **Figure 10: Stress sensitivity of the deformation mechanisms in the Holocene and glacial ice. (a) Strain rates predicted by the dislocation creep mechanism (dotted lines) and GBS-limited creep (continuous lines) at 0.01 MPa (blue), 0.05 MPa (green), 0.10 MPa (red), 0.25 MPa (purple) and 0.50 MPa (orange). For readability, only the results of the micro-scale constant stress model are shown. (b) Plot of Glen's flow law (dotted lines) and the composite flow law (continuous lines). For (a) and (b) the temperature profile and the grain size distribution of the NEEM ice core were used in combination with the flow law parameters in Table 2.**